Structural and Functional Assessment of Perilipin 2 Lipid Binding Domain(s)

by

Charles P. Najt,[1,‡] Joel S. Lwande,[1,‡] Avery L. McIntosh,[‡‡] Subramanian Senthivinayagam,[‡] Shipra Gupta,[‡] Leslie A. Kuhn,[‡,†] and Barbara P. Atshaves[*,‡]

From the Departments of

[‡]Biochemistry and Molecular Biology,

[†]Computer Science and Engineering

Michigan State University,

East Lansing, MI 48824

and

[‡‡]Physiology and Pharmacology

Texas A&M University,

TVMC College Station, TX 77843-4466

Running Title: Plin2 lipid binding domains

[1]Both authors contributed equally to the development of this manuscript. *To whom correspondence should be addressed: Department of Biochemistry and Molecular Biology, Michigan State University, East Lansing, MI 48824. Telephone: (517) 353-5284, FAX: (517) 353-9334, e-mail: atshaves@msu.edu.

Funding Source Statement: This work was supported in part by the U.S. Department of Health and Human Services, National Institutes of Health, grant DK70965 (BPA). Funding to foster this work was also obtained from the Office of the Vice President for Research, the College of Natural Science, and the Department of Molecular Biology and Biochemistry of Michigan State University.

Abbreviations: Plin, Perilipin; ADRP, adipose differentiation-related protein; TIP47, tail-interacting protein 47; PAT, Perilipin/ADRP/TIP47; ACBP, acylCoA binding protein; NBD-cholesterol, [22-(N-(7-nitrobenz-2-oxa-1,3-diazol-4-yl)amino)-23,24-bisnor-5-cholen-3b-ol]; NBD-stearate, 12-N-methyl-(7-nitrobenz-2-oxa-1,3-diazo)aminostearic acid; PDB, Protein Data Bank; HDL, high density lipoproteins; VLDL, very low density lipoproteins; and FRET, fluorescence resonance energy transfer.

Key Words: lipid droplets, ADRP, Plin3, molecular modeling, lipid binding, lipoproteins.

ABSTRACT

Although Perilipin 2 (Plin2) has been shown to bind lipids with high affinity, the Plin2 lipid binding site has yet to be defined. This is of interest since Plin2's affinity for lipids has been suggested to be important for lipid droplet biogenesis and intracellular triacylglycerol accumulation. To define these regions, mouse Plin2 and several deletion mutants expressed as recombinant proteins and in mammalian cells were assessed by molecular modeling, fluorescence binding, circular dichroic, and FRET techniques to identify the structural and functional requirements for lipid binding. Major findings of this study indicate: 1) The N-terminal PAT domain does not bind cholesterol or stearic acid; 2) Plin2 residues 119-251, containing helix α4, the α−β domain, and part of helix α6 form a Plin3-like cleft found to be important for highest affinity lipid binding; 3) Both stearic acid and cholesterol interact favorably with the Plin2 cleft formed by conserved residues in helix α6 and adjacent strands, which is common to all the active lipid-binding constructs; and 4) Discrete targeting of the Plin2 mutants to lipid droplets supports Plin2 containing two independent, non-overlapping lipid droplet targeting domains in its central and C-terminal sequences. Thus, the current work reveals specific domains responsible for Plin2-lipid interactions that involves the protein's lipid binding and targeting functions.

Although the lipid droplet protein perilipin 2 (Plin2, also known as adipose differentiation-related protein, ADRP, or adipophilin) has been shown to play a key role in lipid droplet formation,[1] intracellular triglyceride accumulation,[1-4] and to bind lipids with high affinity,[5-8] little is known regarding the structure or location of its lipid binding site(s). Since Plin2's binding capacity can influence several lipid parameters including fatty acid uptake in a chain length specific manner,[9] HDL-mediated cholesterol uptake/efflux,[8, 10] and VLDL content in mouse models of obesity,[11] this represents a significant gap in knowledge. In fact, a genetic variation in the *Plin2* gene causing a serine to proline mutation (Ser251Pro) resulted in dysregulation of plasma lipid and lipoprotein profiles in humans,[12] possibly due to disruption of helical structure within a putative lipid binding site. As part of the Plin (or PAT, for *p*erilipin/*A*DRP/*T*IP47) family of lipid droplet targeting proteins which includes Plin1/perilipin, Plin2/ADRP, Plin3/TIP47, Plin4/S3-12, and Plin5/OXPAT, Plin2 shares high sequence homology with members of the group (rev in [13]). With Plin1[14] and other lipid droplet-associated proteins such as caveolins,[15] the targeting and anchoring of proteins depends on targeting signals in the form of hydrophobic sequences. These signals were not however, conserved in Plin2,[14] suggesting different lipid droplet targeting mechanisms exist among lipid droplet associated proteins. In support of this, two potential lipid droplet targeting domains in Plin2 were reported that were not hydrophobic in nature.[16, 17] These domains were non-overlapping suggesting that targeting of Plin2 to lipid droplets was controlled by the tertiary structure in which contributing residues were brought together to form the targeting signal.[16, 17] Likewise, the lipid binding site of Plin2 may also be defined by the tertiary structure of the protein and may not be easily described by a linear sequence motif. In keeping with this, there is evidence that binding of cholesterol and other lipids by membrane proteins often occurs in grooves between helices and involves conserved

spatial motifs.[18-21] Based on sequence similarity[22] and predicted structure,[16, 17] several conserved regions within Plin2 have the potential to bind lipids including: 1) a highly conserved N-terminal hydrophobic domain (residues 1-115) known as the PAT domain[22, 23] that is involved in lipid droplet stabilization, lipid accumulation, and proteasomal degradation of Plin2;[23, 24] 2) the N-terminal 11-mer repeating domain located within residues 103-215[25, 26] that is believed to participate with part of the C-terminal domain to regulate secretion of milk lipids by forming an adaptive link between lipid droplets and the plasma membrane;[27] 3) two predicted lipid droplet targeting domains in the middle and C-terminal regions of the protein;[16, 17] and 4) a C-terminal α-β domain and a 4-helix bundle domain reminiscent of the LDL receptor binding domain of apolipoprotein E.[25] The last structure was predicted based on homology between Plin2 and the known crystal structure of the closely related Plin3.[25] In Plin3, the α-β domain and 4-helix bundle fold together into an L-shape, forming a cleft (13 Å at its widest, 18 Å long, and 10 Å deep) with several hydrophobic residues and a deep polar pocket of sufficient size to accommodate lipid ligands and interact with their polar groups. Since Plin2 and Plin3 share 42% overall sequence identity throughout and 35% identity in the C-terminal region (NCBI BLAST), substantial structural similarity is expected. In fact, a comprehensive study has shown that sequences with at least 25% identity over at least 80 residues have backbone structures that overlay closely.[28] Recently, a structural model was presented for Plin2 based on sequence similarity to the known 3-dimensional structures of Plin3, apolipoprotein A1, the signal receiver domain of a putative luxo repressor protein, and dihydroorotate reductase.[29] Work presented here supports that an apolipophorin-like N-terminal domain and a Plin3-like C-terminal domain together can account for the overall tertiary fold of Plin2. Others have noted structural similarities between apolipoprotein A1 and the N-terminal domain of Plin proteins. Both contain

11-mer repeats (located within helix α4 and the α–β domain in Plin2) that are found in other lipid- or membrane-associated proteins including phosphate cytidyltransferases and synucleins,[30] suggesting these domains may serve as lipid interacting sites in these proteins.

The present investigation was undertaken to examine the structure and location of the Plin2 lipid binding site(s) within conserved domains by characterizing Plin2 and several deletion mutants using molecular modeling, fluorescence binding, circular dichroism, and FRET techniques. Evidence is provided that lipid binding by Plin2 does not require the full-length protein, but instead employs residues from two helical bundle domains for highest affinity lipid binding and targeting to lipid droplets, activities that are dependent on strong Plin2-lipid or Plin2-membrane interactions. Crucial residues within these domains are 119-251, a region that contains helix α4, the α–β domain (α5, β3), and part of helix α6, included in the cleft region. Residues within ConSurf analysis shows that surface-exposed residues within the cleft are highly conserved and likely to be functionally important. Furthermore, flexible docking of stearic acid and cholesterol into this region indicates favorable interactions with both ligands and the cleft formed from a polar pocket with surrounding hydrophobic residues. Since mutations in this region of Plin2 resulted in dysregulation of plasma lipid and lipoprotein profiles in humans,[12] study of the functional importance of this area is warranted.

MATERIALS AND METHODS

Materials. Cholesterol and stearic acid were purchased from Sigma (St. Louis, MO). NBD-Cholesterol and NBD-stearic acid were obtained from Molecular Probes (Eugene, OR). Expression vector pQE9-His was purchased from Addgene (Cambridge, MA). CFP-fusion protein expression vector pECFP-N1 was purchased from BD Biosciences (BD Biosciences Clontech, Palo Alto, CA). Ni-NTA resin and M15 cells for protein expression were obtained from Qiagen (Chatsworth, CA). Rabbit anti-Plin2 polyclonal anti-body was prepared as described.[31] Lipofectamine 2000 was purchased from Life Technologies-Invitrogen (Carlsbad, CA).

Buffers. Buffer A contained 50 mM Na_2HPO_4 (pH 8.0), 300 mM NaCl, and protease inhibitors (1 tablet per 50ml). Buffer B contained 20 mM Tris-HCl (pH 7.9), 100 mM Na_2HPO_4, 500 mM NaCl and 20 mM imidazole and 6M guanidine hydrochloride. Buffer C contained 20 mM Tris-HCl (pH 7.9), 500 mM NaCl, 20 mM imidazole, and 6 M urea. Buffer D was Buffer C at pH = 5.9. Buffer E was 10 mM Tris-HCl (pH 7.5), and 150 mM NaCl. Buffer F contained PBS, 2 mM EDTA, 10 mM DTT, and protease inhibitors. Buffer G contained PBS, 10 mM DTT, 0.1% SDS and 10% glycerol. Buffer H was PBS, 10 mM DTT and 2 M urea. Buffer I was Buffer H in 8 M urea. Buffer J was Buffer E at pH 8.3 plus 20mM imidazole. Buffer K was Buffer J at pH 7.5. Buffer L was Buffer E plus 50mM EDTA.

Plasmids. The full coding sequence of mouse Plin2 cDNA was cloned into pQE9-His vector (Origene, Rockville, MD) following standard procedures. Unique restriction sites *Bam*HI and *Hin*dIII were introduced by PCR amplification with the following forward and reverse primers: Plin2-forward, 5'-CAC GGA TCC ATG GCA GCA GCA GTA GTA GAT CCG CAA C -3'and Plin2-reverse, 5'-GTG AAG CTT TTA CTG AGC TTT GAC CTC-3'. The forward primer was

designed with a silent mutation where guanine was replaced by adenine in the Plin2 sequence to remove a *Bam*HI site located within the first 18 bp of the Plin2 gene. By cloning Plin2 cDNA into the pQE9-His vector, an N-terminal His-Tagged fusion protein was formed upon expression that allowed recombinant protein to be purified using Ni-NTA based affinity chromatography. Expression plasmids for the deletion mutants were generated from the above construct by site-directed mutagenesis as described elsewhere [32] using the following primers: Plin2-C1 forward, 5'-CAT CAC GGA TCC ATG ACG ACT ACC ATG GCT GGA GCC-3'; Plin2-C1 reverse, 5'-AGC CAT GGT AGT CGT CAT GGA TCC GTG ATG GTG ATG-3'; Plin2-C2 forward, 5'-CAT CAC GGA TCC ATG GTC CAC CTG ATT GAA TTC GCC-3'; Plin2-C2 reverse, 5'-TTC AAT CAG GTG GAC CAT GGA TCC GTG ATG GTG ATG-3'; Plin2-N1 forward, 5'-GAT GTG ACG ACT TAA AAG CTT AAT TAG CTG AGC-3'; Plin2-N1 reverse, 5'-CTA ATT AAG CTT TTA AGT CGT CAC ATC CTT CGC-3'; Plin2-N2 forward, 5'-ACC ATT TCT CAG CTC TAA AAG CTT AAT TAG CTG AGC-3'; Plin2-N2 reverse, 5'-CTA ATT AAG CTT TTA GAG CTG AGA AAT GGT CTC CTG-3'. Plin2-I was made using Plin2-C1 as the template DNA and the primers used for creating Plin2-N2. The resulting plasmids were sequenced to ensure fidelity and identity.

Expression and purification of recombinant proteins in *Escherichia coli* cells.

Recombinant Plin2 and the deletion mutants were overexpressed in *E. coli* host strain M15 and grown at 37 ^{o}C in 1 liter cultures containing 2X-YT medium with 100 µg/mL ampicillin until OD_{600} = 0.8, followed by induction with IPTG (1 mM). After 1 hour, cells were harvested by centrifugation (4 ^{o}C for 30 min at 3500 g). For purification of Plin2, Plin2-I, Plin2-N1, and Plin2-N2, pelleted cells were resuspended in Buffer A then sonicated. Lysates were centrifuged at 4 ^{o}C for 15 min at 25000 g and the pellet was solubilized in Buffer B and applied to a Ni-NTA

column equilibrated in Buffer B. The column was sequentially washed with buffers B, C and D, and E. The protein was eluted using Buffer L and then checked for purity by SDS-PAGE analysis. For deletion mutants Plin2-C1 and Plin2-C2, the pelleted cells were resuspended in Buffer F, sonicated, and centrifuged at 4 ^{o}C for 15 min at 25000 g. The resulting pellet was washed 2x each with buffers G and H, solubilized in Buffer I, and centrifuged at 4 ^{o}C for 15 min at 25000 g. The supernatant was then sequentially dialyzed against PBS containing 10 mM DTT in decreasing concentrations of urea (6 M, 5 M, and 4 M urea). The protein in 4 M urea was then loaded onto a Ni-NTA column equilibrated in Buffer J. The column was then sequentially washed with the buffers J and K, and then eluted with Buffer L. Analysis by SDS-PAGE and Western blotting as described in [4] allowed assignment of protein purity.

Plin2 structural prediction and analysis. The Hopp and Woods hydropathy analysis method[33] (web server: http://www.vivo.colostate.edu/molkit/hydropathy/index.html) was used to predict hydrophilic and hydrophobic segments within Plin2 based on a hydrophilicity index assigned to the amino acids, averaged over six successive residues. The PAT domain and two lipid droplet targeting domains in Plin2 were previously described in [17, 24, 26]. The secondary structure of Plin2 was predicted by the PredictProtein server at http://www.predictprotein.org.[34] This method has greater than 72% accuracy, on average, in assigning α-helical, β-strand (extended) or loop conformation to protein residues. Secondary structural predictions of the Plin2 N-terminal region (residues 1-171) were consistent with further analysis by PSIPRED,[35, 36] SAM,[37] and SABLE2.[38] Based on their significant (35%) sequence identity, the Plin2 C-terminal domain structure was modeled by homology to the structure of residues 209-431 in Plin3[25] from Protein Data Bank entry 1SZI[39] by using Modeller,[40, 41] as implemented in the ModWeb webserver (salilab.org/modweb). Given the absence of close homologs of known structure to the

Plin2 N-terminal region, this sequence was submitted for analysis by the Pcons fold recognition web server (http://pcons.net/) to identify the 3-dimensional structural fold providing the most compatible amino acid environments and secondary structures. By comparing the top-scoring predictions from eleven different 3-dimensional modeling methods (Pcons, Pmodeller, PconsM, blast, forte, fugue, hhpred2, nfold, rpsblast, sam-t02 and sam-t08), Pcons selected the structural model for the N-terminal Plin2 region showing the highest degree of structural consensus among the results. The degree of amino acid conservation within 38 homologs of the C-terminal domain of ADRP was assessed by ConSurf (http://consurf.tau.ac.il/), which automatically detects homologs, performs multiple sequence alignment, and maps amino acid conservation values onto the structure.[42, 43] Molecular graphics figures were rendered using PYMOL (Schrödinger, LLC).[31] Stearic acid interactions with the modeled Plin2 C-terminal domain were assessed by extracting the 3-dimensional structure of stearic acid from the PDB X-ray structure 1HMT.[44] Partial charges were assigned to its atoms with Molcharge v. 1.3.1 software from OpenEye Scientific Software (http://www.eyesopen.com; Santa Fe, NM). Low-energy (favorable) flexible conformations of highly flexible stearic acid were then generated by using Omega2 v. 2.3.2 (also from OpenEye Scientific Software). Similarly, the 3-dimensional structure of cholesterol (residue 3001D) was extracted from PDB entry 3KDP.[45] Partial charges were assigned with Molcharge, and low-energy conformations of the cholesterol hydrophobic tail were sampled with Omega2. The stearic acid and cholesterol conformers were evaluated for their ability to interact favorably with the conserved cleft in the 3-dimensional model of the C-terminal domain structure of Plin2 by using SLIDE version 3.3.5 software to dock each conformer of stearic acid or cholesterol into the cleft between the α-β domain and 4-helix bundle, and selecting the orientation and conformation with the most favorable predicted $\Delta G_{binding}$ to Plin2, as assessed by

SLIDE AffiScore. SLIDE models side-chain flexibility in both molecules during docking.[46]

Cells culture and transfections. Mouse L cell fibroblasts expressing CFP-labeled Plin2 and the deletion mutants were generated as described in[4] using mammalian expression vector pECFP-N1 and unique restriction sites (*Xho*I, *Kpn*I) introduced by PCR. Resulting expression plasmids were sequenced to verify identity and fidelity and then stably transfected into L cells using Lipofectamine 2000 from Life Technologies (Grand Island, NY) according to the manufacturer's instructions. Clones surviving selection with G418 were cell-sorted for strong CFP signal under sterile conditions using an INFLUX cell sorter (BD scientific, Palo Alto, CA) and screened by Western blot analysis and fluorescence imaging to ensure stable expression of CFP-labeled protein. Mock transfectants (clones transfected with vector DNA without insert) were generated in parallel and were designated as controls.

Urea denaturation studies. To show the effects of protein unfolding on Plin2 tryptophan residues, protein-denaturation studies in the presence of urea were performed as described in [47]. In brief, the intrinsic tryptophan fluorescence (excitation 295 nm, emission 300 to 400 nm) of three Plin2 tryptophans located at positions 283, 286, and 398 was collected using a Cary Eclipse fluorescence spectrophotometer (Varian, Walnut Creek, CA) at constant temperature (25^0C) before and after addition of increasing amounts of urea (up 6 M) to Plin2 (100nM) in 10 mM NaH_2PO_4, pH 7.5. Samples were allowed to equilibrate 2 minutes after addition of each urea aliquot. Data was corrected for background scatter originating from the buffer and analyzed to graphically show the tryptophan fluorescence spectrum at increasing urea concentrations and the percent fluorescence remaining after each addition.

Intrinsic tryptophan fluorescence binding studies. The binding of cholesterol and stearic acid to Plin2 was examined by measuring the fluorescence quenching of Plin2 tryptophan

residues after addition of ligand as described in [48, 49]. In brief, the intrinsic tryptophan fluorescence of Plin2 (100 nM in 10 mM NaH_2PO_4, pH 7.5) was monitored from 300 to 400 nm after excitation at 295 nm (to minimize interference from Plin2 tyrosine fluorescence) both before and after addition of increasing increments of cholesterol or stearic acid (up to 100 nM) using a Cary Eclipse fluorescence spectrophotometer. Data was corrected for background scatter originating from the buffer and increasing ligand without protein present. The intrinsic tryptophan fluorescence in the presence of different concentrations of ligand was plotted as the maximum fluorescence difference ($\Delta F = F_o - F$) vs. ligand concentration to yield a saturation curve where F and F_o were the measured fluorescence emission intensity of the protein solution in the presence and absence of ligand, respectively. The dissociation constant K_d was determined from the double reciprocal plot of the saturation curve. Linear regression of 1/[1-(F/Fmax)] versus [ligand]/(F/Fmax) yielded a slope = 1/ K_d and ordinate intercept = nE_o/ K_d where F represented fluorescence intensity at a given concentration of ligand, Fmax was the maximal fluorescence, [ligand] was the ligand concentration, E_o was the protein concentration, and n equaled the number of ligand binding sites.

NBD-labeled ligand binding assays. Since not all of the deletion mutations contained tryptophan residues, a fluorescent ligand binding assay was developed using NBD-Cholesterol and NBD-stearic acid as described in [5-8]. In brief, NBD-labeled lipids were added incrementally (0-300 nM) to proteins (Plin2, ACBP, or Plin2 deletion mutants) at 100 nM in phosphate buffer (10 mM, pH 7.5). Samples were allowed to mix 2-5 min after each addition before exciting at 469 nm. Fluorescence emission spectra were recorded from 490 to 600 nm and integrated. Data was corrected for both background scatter originating from the buffer and increasing ligand without protein present. A saturation curve developed by plotting fluorescence intensities vs.

ligand concentration and the double reciprocal plot of this curve allowed determination of K_d as discussed previously.

Co-localization studies. To show the ability of Plin2 and the deletion mutants to target to lipid droplets, co-localization studies were performed as described in [4, 31] with cells expressing full length Plin2 or one of the deletion constructs. Cells seeded at a density of 50,000 cells/well in 4-well chamber slides (EZ Slide, Millipore, Billerica, MA) were treated overnight with oleic acid (100μM) 4-5 hrs after plating. After 16 hrs, cells were incubated with NBD-Cholesterol (2μM) for 2 hours, then fixed in 3.7% formaldehyde for 20 min at room temperature followed by washing (3x) with PBS. The cells were then blocked with 2% BSA and incubated with rabbit anti-CFP antibody (1:50) for 1 hr at room temperature. Since the transfected cells express CFP-labeled proteins (as described above), anti-CFP was used in place of anti-Plin2 to discriminate endogenous Plin2 from the transfected mutant proteins. After extensive washing, cells were incubated with Cy5 labeled anti-rabbit secondary antibody (1:100) in 2% BSA for 1 hr. Cells were washed with PBS and mounted with coverslips using fluorogel mounting medium (Electron Microscopy Science, Hatfield, PA). As a control, cells were also labeled with the Cy5-labeled secondary antibody alone. Images were acquired sequentially on an Olympus FluoView 1000 Laser Scanning Confocal Microscope (Olympus Inc, Center Valley, CA) equipped with an IX81 automated inverted microscope and operated with Fluoview software. Fluorescence emission was detected using 488 nm excitation and 500/100 band path emission filter for NBD-Cholesterol (green channel) and 635 nm excitation with a 725/30 band path filter for the Cy5 emission (red channel). To minimize photobleaching, samples were exposed to the light source for minimal time periods. Image files were analyzed using Metamorph software (West Chester, PA). Images derived from the red and green channels were combined and appeared as yellow to

orange where superimposition of images derived from the red and green channels overlapped.

Fluorescence resonance energy transfer microscopy. Acceptor photobleaching experiments were performed following methods in [4, 50] on cells labeled as described above by measuring the fluorescence emission of the NBD donor through the 500/100 nm filter upon excitation at 488nm both before and after photobleaching of the Cy5-acceptor excited at 635nm. Control experiments were performed to limit interference from non-specific fluorescence including: 1) Imaging non-labeled cells to determine auto-fluorescence in the green channel (NBD) while maintaining maximum dynamic range; 2) Adjusting the gain and black levels in the red channel after excitation at 635nm to limit fluorescence bleed-through into the green channel; 3) Photobleaching NBD-labeled donor cells without Cy5 present to check for non-specific fluorescent increases in the donor channel to ensure that the donor intensity was not affected by bleaching the cells; and 4) Leaving one or two cells unbleached during the FRET experiment to serve as in-field bleaching control. To calculate the FRET efficiency (E), representing the efficiency of energy transfer between donor and acceptor, the following equation was used: $E = 1-(I_{DA}/I_D)$ where I_{DA} is donor fluorescence intensity before acceptor photobleaching and I_D is the donor fluorescence intensity after acceptor photobleaching. An average E value was calculated from the NBD fluorescence emission increase after photobleaching. The intermolecular distance R between NBD-label and the Cy5-labeled Plin2 was calculated from the equation $E = 1/(1-(R/R_o)^6)$, where E was experimentally determined and R_o the Foster radius for the NBD-Cy5 FRET pair (56 Å).

Circular dichroic analysis of secondary structure. The far UV circular dichroic (CD) spectra of each protein was measured in phosphate buffer (10 mM NaH_2PO_4, pH 7.5 with 10 mM NaCl) in the presence and absence of ligand (cholesterol or stearic acid) to a final concentration

of 5 μM. Experiments were performed at 25ºC in a 1 mm path length cuvette using a JASCO J-815 CD spectrometer (JASCO Analytical Instruments, Easton, MD). Experiments with ligand were allowed to incubate for 2-5 min prior to each scan to allow maximal protein-ligand interaction. CD spectra were recorded from 270 to 190 nm at a scan rate of 50 nm/minute with a time constant of 1 s and bandwidth of 2 nm. For each experiment, 10 iterations were performed in triplicate. Secondary structure analysis was carried out using the CDSSTR analysis program[51] with results reported as percentages of regular α-helices, distorted α-helices, regular β-strands, distorted β-strands, turns and unordered structures. In a separate experiment, measurements on purified recombinant Plin2 were performed at 5ºC, 25ºC, and 40ºC to determine the dependence of secondary structure on temperature.

Statistics. All values were expressed as the means $\pm$ S.E. Statistical analyses were performed using Student's t test or one-way ANOVA with Newman Keuls post-hoc test (GraphPad Prism, San Diego, CA) to determine statistical significance. Values with $P< 0.05$ or less were considered significant.

RESULTS

Prediction of Plin2 secondary structure and conserved domains. To understand how ligand binding relates to structure, the secondary structure of Plin2 was predicted using several prediction programs including PredictProtein,[34] PSIPRED,[35, 36] SAM,[37] and SABLE2.[38] Results from these programs indicated that the secondary structure of Plin2 is mostly α-helical in nature (9 α-helices) with 5 β strands inter-connected by random coils (Fig. 1A). The Plin2 N-terminal region contains 2 β-strands (β1, β2) and 4 α-helices (α1, α2, α3, and α4). Based on homology to the C-terminal domain of the crystal structure of Plin3, the Plin2 C-terminal region is predicted to contain an α−β domain (α5, β3), a 4-helix bundle (α6- α9), and 2 β-strands (β4, β5) that together form a deep cleft that is conserved in the perilipin family and large enough to bind lipids.[25] In addition, several conserved regions have been identified within Plin2 including a highly conserved hydrophobic domain within the N-terminal region (residues 1-115) known as the PAT domain (Fig. 1B), which was shown to participate in the stabilization and accumulation of lipid droplets and to determine proteasomal degradation of Plin2;[22-24] an 11-mer repeating unit of unknown function within residues 103-215 (Fig. 1A); and two lipid droplet targeting domains[16, 17] located in the middle and C-terminal regions (Fig. 1B) that participated with part of the C-terminal domain to regulate secretion of milk lipids.[13, 27] Alternating patterns of hydrophobic/hydrophilic segments are observed in Plin2 (Fig. 1C) and Plin3 (Fig. 1D) over the N-terminal PAT domain and 11-mer repeat region from patterns of hydrophobicity predicted using the method of Hopp and Woods.[33] In keeping with the high degree of homology shared between these proteins, similar hydrophobic characteristics were observed for both Plin2 and Plin3. Large segments of hydrophobic sequence conducive to membrane targeting were not observed with either protein, suggesting that regions within the protein come together spatially to

form larger recognition surfaces for hydrophobic ligands including the membrane itself.

To assess the lipid binding affinities of these regions, Plin2 and several Plin2 deletion mutants including Plin2-C1, Plin2-C2, Plin2-I, Plin2-N1, and Plin2-N2 (Fig. 1) that contain select regions within Plin2 with the potential to bind lipids were expressed in *E. coli* and purified as recombinant proteins. The deletion mutants included regions containing the PAT domain,[23] one or two of the lipid droplet targeting domains,[16, 22] or the central alpha/beta domain residues near the cleft in the C-terminal region[25] (Fig. 1E). Plin2-C1 included the two potential lipid droplet targeting domains and the corresponding region of Plin3 that was resolved by X-ray crystallography.[25] Deletion mutant Plin2-C2 was similar to Plin2-C1 but retained only one of the lipid droplet targeting domains and 9 of the 15 amino acid residues in the alpha/beta domain found in the cleft region (Fig. 1E). Plin2-I covered the entire Plin2 sequence except the central region (residues 172-218), deleting the α-β domain and two cleft residues. Plin2-N1 contained only the PAT domain. Deletion mutant Plin2-N2 included the PAT domain,[23] one of the potential lipid droplet targeting domains, and 6 of 15 cleft residues.

Effect of urea and temperature on Plin2 structure: Intrinsic tryptophan fluorescence quenching and CD analysis. Recombinant full length Plin2 protein was overexpressed and purified as described in the Methods section (see Supplement Fig. 1). To determine if the recombinant Plin2 protein was conformational and functionally intact, two distinct experiments were performed. First, to show the effects of protein unfolding, Plin2 was tittered against increasing amounts of urea, up to 6 M. Protein unfolding was monitored via tryptophan fluorescence, as described in [47] and in the Methods section. Tryptophan fluorescence, in contrast to tyrosine fluorescence, is sensitive to solvent polarity, therefore it can be used as a measure of protein folding.[52] Plin2 contains three tryptophan residues in the C-terminal region at positions

283, 286, and 398. More importantly, the tryptophan residues are located in the 4-helix bundle of the predicted binding region of the protein. Analysis of the Plin2 tryptophan fluorescence emission collected from 300 nm to 400 nm showed the refolded full length Plin2 protein exhibited a typical emission spectra with maxima at 327 nm (Fig. 2A), indicating a blue-shift relative to tryptophan in water where the fluorescence maximum is 348 nm.[53] Addition of increasing concentrations of urea (up to 6 M) resulted in fluorescence quenching of one or more of the three tryptophan residues (Fig. 2A). A red-shift in the emission maxima to 332 nm at 4.6 M urea was observed, indicating increased exposure of the residues to the hydrophilic solvent. At 6 M urea, only 22% of the initial tryptophan fluorescence remained indicating substantial exposure of the tryptophan residues to the solvent. It is this 78% decrease in tryptophan fluorescence and red shift that is indicative of denaturation of the refolded protein (Fig. 2B).

Second, to show the effects of protein unfolding on Plin2 secondary structure, changes in the CD spectra at increasing temperatures was examined. At room temperature (25^0C) recombinant Plin2 exhibited a double minimum at ~208 and 222 nm signifying substantial amounts of α-helices were present (Fig. 2C). However, the molar ellipticity at 208 nm was lower than at 222 nm suggesting a subtle influence of random coils and β-sheets. Upon lowering the temperature to 5^0C, the minima at 208 nm and 222 nm were intensified, consistent with slower conformational transitions and enhanced resolution. In contrast, at 40^0C the protein began losing its secondary structure as the peak intensities approached zero molar ellipticity (Fig. 2C). Results from these studies indicated that Plin2 tryptophans in the refolded protein were sensitive to urea denaturation. Moreover, CD analysis of the secondary structure of the refolded protein was consistent with predictions and exhibited enhanced resolution at lower temperatures but destabilization when temperatures were increased above room temperature.

Tryptophan quenching binding studies: Full length Plin2 binds cholesterol and stearic acid with high affinity. The binding affinity of the full length Plin2 protein for cholesterol and stearic acid was determined by measuring changes in the intrinsic tryptophan fluorescence of Plin2 upon ligand addition. Fluorescence quenching of one or more of the three tryptophan residues located in the C-terminal 4-helix bundle resulted in a decrease in fluorescence signal intensity when ligand was added. A plot of the change in fluorescence intensity (F_0-F) as a function of ligand concentration showed saturable binding curves for cholesterol (Fig. 3A) and stearic acid (Fig. 3B) where F and F_o were the measured fluorescence emission intensity of the protein solution in the presence and absence of ligand, respectively. The dissociation constant K_d was determined from the double reciprocal plot of this curve with s 1/[1-(F/Fmax)] versus [ligand]/(F/Fmax) yielding a linear regression line (Fig 3, insets) where the slope of the line was $1/ K_d$ and the ordinate intercept, nE_o/ K_d. Analysis of multiple plots revealed that Plin2 bound cholesterol and stearic acid with a K_d of 7 $\pm$ 1 nM and 80 $\pm$ 9 nM, respectively at a single site that was not necessarily the same for each ligand. Thus, Plin2 exhibited very high affinity for cholesterol and less so for stearic acid, consistent with values obtained from previous studies,[5, 6, 8] indicating that the purified recombinant Plin2 protein contained an active ligand binding site.

NBD-labeled binding studies: Plin2 and deletion mutants bind cholesterol and stearic acid with selective affinity. Recombinant Plin2 deletion mutants were overexpressed and purified as described in the Methods section (see Supplement Fig. 1). To establish the ability of Plin2 and the deletion mutants to bind lipids such as cholesterol and stearic acid, NBD-labeled lipid binding assay were performed as described in [5-8]. The NBD-fluorophore in NBD-lipids was sensitive to environmental hydrophobicity and therefore provided a useful tool to determine ligand binding affinity. NBD-cholesterol showed minimal fluorescence in aqueous buffer with an

emission maximum (λmax) equal to 545nm. Addition of Plin2 or the deletion mutant proteins resulted in increased fluorescence with shifts in λmax to blue wavelengths (0-5 nm) indicating binding of the probe to a site increasingly more hydrophobic than the aqueous buffer (Table 1). With full length Plin2, a plot of the NBD-cholesterol fluorescence maximum at 543 nm versus increasing NBD-cholesterol concentration showed a monophasic binding curve reaching saturation (Fig. 4A). A double reciprocal plot of this curve was linear (Fig. 4A, inset) and yielded a $K_d = 11 \pm 2$ nM (Table 1), in keeping with results from the tryptophan quenching studies (Fig. 3A) and with previous reports.[5, 8] In comparison, deletion mutants Plin2-C1 (Fig. 4B), Plin2-I (Fig. 4F), Plin2-N2 (Fig. 4E), and Plin2-C2 (Fig. 4C) showed significantly less affinity for NBD-cholesterol with $K_d = 48 \pm 3$ nM, 34 ± 4 nM, 50 ± 6 nM, and 98 ± 10 nM, respectively (Table 1). Most interestingly, deletion mutant Plin2-N1 (Fig. 4D) did not bind NBD-cholesterol, showing little to no increase in fluorescence over the buffer control. This last result indicated that the cholesterol binding site for Plin2 did not reside within the PAT domain.

With NBD-stearic acid binding to full length Plin2, $K_d = 121 \pm 12$ nM, consistent with results from the tryptophan quenching studies (Fig. 3B) and from previous reports.[5, 6] The NBD-labeled probe was minimally fluorescent in buffer but showed increased fluorescence once bound in the hydrophobic environment of protein binding pocket. As with NBD-cholesterol, a plot of the NBD-stearate fluorescence maximum (544 nm) versus increasing NBD-stearate concentration showed a monophasic binding curve reaching saturation (data not shown). Similar saturation curves were observed for all the deletion mutants that bound NBD-stearic acid, although the emission maxima were different (Table 1), indicating differences in the hydrophobicity of the ligand binding pocket. For deletion mutants Plin2-I and Plin2-C1, the maximal intensity of NBD-stearate emission (λmax) blue-shifted from 544 nm to 540 nm and

538 nm, respectively, indicating the probe was in a more hydrophobic environment. These results were consistent with the high affinity binding observed with these deletion mutants where K_d = 90±7 nM and 69±7 nM, respectively. No shift in the fluorescence maximum was observed with deletion mutant Plin2-C2 which exhibited significantly less affinity for NBD-stearate with K_d = 160 ± 35 nM (Table 1). Interestingly, despite high affinity binding of NBD-stearic acid to Plin2-N2 a red shift in the λmax was observed, indicating the probe was in a relatively less hydrophobic environment. Lastly, Plin2-N1 did not bind NBD-stearic acid (Table 1), consistent with results with NBD-Cholesterol, suggesting this mutant does not contain a lipid binding site.

The specificity of the fluorescence binding assay was also studied by performing the NBD-Cholesterol binding assay with acyl CoA binding protein (ACBP), a cytosolic lipid binding protein that exclusively binds long-chain fatty acyl CoA[54] but not cholesterol or fatty acids.[55] When increasing concentrations of NBD-cholesterol were added to ACBP in solution, no increase in fluorescence was observed after background subtraction, indicating that ACBP did not bind NBD-cholesterol. The data was plotted as a function of NBD-cholesterol maximal intensity at 538 nm versus increasing NBD-labeled ligand concentration to yield a line with scattered points (Fig 4G), a further indication of no binding. These results suggest NBD-cholesterol did not enter the ACBP binding pocket and support the specificity of Plin2 for NBD-cholesterol was valid. Similar results were observed with NBD-stearic acid where ACBP exhibited little to no affinity for the fluorescent probe (data not shown).

Intracellular targeting and FRET analysis. The extent of Plin2/lipid interactions on the lipid droplet surface were determined in a series of experiments using NBD-labeled cholesterol in colocalization and FRET assays. First, co-labeling of NBD-cholesterol with Cy5-labeled Plin2 overexpressed in L cells was accomplished as described in the Methods section and repeated

with each deletion mutant. Simultaneous acquisition of multiple confocal images of NBD-cholesterol co-labeled with Cy5-proteins revealed the following expression clones targeted to lipid droplets: Plin2 (Fig. 5A), Plin2-C1 (Fig. 5B), Plin2-C2 (Fig. 5C), and Plin2-I (Fig. 5F). In contrast, expression clones Plin2-N1 (Fig. 5D) and Plin2-N2 (Fig. 5E) showed little to no targeting to lipid droplets. Second, in expression clones that targeted to lipid droplets, FRET analysis was performed as described in previous work[4, 50] to determine the extent of interaction between NBD-cholesterol and the Cy5-labeled proteins. FRET estimates intermolecular distances between molecules to within 10-100 Å, thus allowing detection of direct interactions at the molecular level. FRET was observed between NBD-Cholesterol and Cy5-labeled Plin2 and the mean distance *R* between the pair was calculated to equal 77 $\pm$ 4 Å, indicating close proximity (Table 2). FRET efficiency (*E*), a measure of the extent of probe overlap, was determined as 25 $\pm$ 5, values consistent with efficient overlap of electronic states and direct interaction of NBD-cholesterol and Plin2 on the lipid droplet surface. In similar fashion, FRET was performed with NBD-cholesterol and the Cy5-labeled deletion mutants to show FRET occurred between the NBD-labeled ligand and the following deletion mutants: Plin2-C1, Plin2-C2, and Plin2-I with R values ranging from 85-96 Å (Table 2). No FRET was observed with Plin2-N1 or Plin2-N2. Taken together, these findings were consistent with results from the binding studies and indicated that Plin2 and several of the deletion mutants directly interacted with NBD-Cholesterol on the lipid droplet surface.

Circular dichroic analysis of ADRP and deletion mutants. To further examine how structure affects function, the secondary structures of Plin2 and the deletion mutants were analyzed by circular dichroism (CD) both with and without ligand (cholesterol and stearic acid). In absence of ligand, the CD spectrum for full length Plin2 (Fig. 6A, solid line) showed a double

minimum at ~208 and 222 nm signifying the presence of substantial amounts of α-helices. The molar ellipticity was slightly lower at 208 nm than at 222 nm however, indicating a significant amount of unordered structure or random coil. A similar trend was visible in the spectra for Plin2-N1 and Plin2-N2 before addition of ligand (Fig. 6D and 6E, solid lines). In contrast, the CD spectra for deletion mutants Plin2-C1, Plin2-C2 and Plin2-I (Fig. 6B, 6C and 6F, solid lines) showed a fairly well balanced molar ellipticity at both wavelengths along with a strong positive peak at 190nm-200nm, indicating that these mutants had less unordered structure and retained strong α-helical character. These results were supported when the data was analyzed using CDSSTR software. Quantitative analysis of multiple CD spectra revealed that deletion mutants Plin2-C1, Plin2-C2 and Plin2-I exhibited the lowest proportion of unordered structure (29%, 29%, and 31%, respectively) and high α-helicity (Table 3). Similar results were shown by SELCON2 analysis (data not shown).

Further analysis of the secondary structure of Plin2 showed that Plin2 contained 21.8% α-helices and 24.5% β-strands based on analysis by CDSSTR analysis (Table 3) with similar results observed with SELCON3 analysis (data not shown). A comparison of the secondary structure of Plin2 to that of each deletion mutant showed that Plin2-C1 and Plin2-C2 had a higher percentage of α-helices (regular and distorted) than Plin2. These results were consistent with secondary structure predictions (Fig. 1A) since Plin2-C1 contained the 4-helix bundle (α6, α7, α8, α9) and Plin2-C2 contained α7, α8, α9, giving them the highest α-helical percentage within the group. In contrast, the other three deletion mutants; Plin2-I, Plin2-N1, and Plin2-N2 exhibited less α-helical structure than full length Plin2 based on both methods of analysis with results showing a respective 16.4%, 10.5%, and 16.5% α-helical structure (regular and distorted). The percentage of β-sheets (regular and distorted) was also significantly higher in Plin2 (24.5%)

when compared to Plin2-C1 (11.5%) and Plin2-C2 (19.1%) but significantly less than Plin2-I (30.2%), Plin2-N1 (40%), or Plin2-N2 (27.2%). Results from CDSSTR analysis showed that Plin2 had significantly more β-turns (21.8%) than Plin2-C2 (19.1%) but less than Plin2-N2 (23.4%). There were no significant differences between Plin2-C1, Plin2-I (19.3%) and Plin2-N1. In summary, in the absence of ligand, the C-terminal region of Plin2 (residues 119-436) exhibited a strong α-helical character with less unordered structure as compared to the full length protein or mutants containing the N-terminal region (residues 1-119). Alternatively, the N-terminal region of the protein contained significantly more unordered structure than the C-terminal region.

The effect of ligand binding on secondary structure was also examined. The addition of cholesterol (Fig. 6A, closed circles) and stearic acid (Fig. 6A, open circles) altered the shape of the CD spectrum of full length Plin2, intensifying the minima at 208 nm with cholesterol but diminishing the peak when stearic acid was present. These alterations were reflected by significant changes in the percent composition of α-helical structures where an increase and decrease respectively, was observed when cholesterol and stearic acid were added to the protein. With the deletion mutants, subtle changes in the CD spectra were also observed upon addition of ligands. As with the full length protein, the CD spectrum of Plin2-C1 showed a significant increase in the intensity of the 208 nm minimum when cholesterol was added but a significant decrease upon addition of stearic acid, reflecting significant increases in both disordered helices and unordered structures while decreasing the percentage of β-sheets (Fig. 6B, Table 3). Subtle conformational changes in the CD spectra were also observed with Plin2-C2, Plin2-I, and Plin2-N2 upon ligand addition, reflecting significant changes in percentage of α-helices and β-sheets based on CDSSTR analysis (Table 3). All three mutants exhibited significant decreases in α-

helical structure when cholesterol was added, concomitant with significant increases in β-sheet and unordered structure (Table 3). In summary, the CD results were consistent with the predicted secondary structure (Fig. 1) and indicated that several of the proteins were sensitive to ligand binding. Lack of conformational change upon ligand binding with deletion mutant Plin2-N1 was consistent with results from the binding studies which indicated that this mutant did not bind cholesterol or stearic acid. Interestingly, the decrease in signal, along with the increase in unordered structure upon addition of stearate was indicative of a more flexible binding pocket that does not enhance the secondary structure of Plin2. Conversely, addition of cholesterol enhanced CD signal and increased the percentage of α-helical character. This increase in structured secondary structure suggests that binding of cholesterol was dependent on a defined secondary structure.

The tertiary structure of the Plin2 C-terminal domain defines a cleft that can interact favorably with stearic acid and cholesterol. The tertiary structure of Plin2 (Fig. 7A) was modeled by using two comparative modeling approaches. Homology modeling by Modeller [40] (web server: http://salilab.org/modweb) was employed for the C-terminal domain based on its sequence similarity to Plin3, since this technique provides the most accurate structural models. Modeller constructed a homology model of the structure of C-terminal residues 190-409 of murine Plin2 (Fig. 7A) based on its alignment with murine Plin3 (also known as TIP47) with 38% sequence identity, well above the 25% threshold required for confident homology modeling.[28] In the absence of a structural template with high enough sequence similarity to the N-terminal region of Plin2 to allow homology modeling, the next most accurate approach, fold recognition, was used. This approach defines the best-matching structural template in the Protein Data Bank (PDB) based on the compatibility of the query sequence with the primary and

secondary structure of the NMR or crystal structure being evaluated as a template, and the favorability of the 3-dimensional chemical interactions of each residue with its neighbors when modeled using that particular 3-D structure. The Pcons.net (http://pcons.net) server was used to model residues 1-171 of murine Plin2 based on the consensus of predicted structures from 11 different fold recognition methods. Of the 10 highest-consensus structural models provided by Pcons, two corresponded to functionally relevant apolipoprotein structures that form compact α-helical bundles: apolipophorin III (PDB entry 1AEP, residues A6-A158);[56] and apoliprotein A-I (PDB entry 2A01, residues A44-A187.[57] The apolipophorin-based model for Plin2 was chosen based on having higher sequence identity (20%, relative to 10% sequence identity for apolipoprotein A-I). Additionally, the matched region of Plin2 corresponds to the entire helical bundle structure of apolipophorin, including a fifth, irregular helix, as shown in yellow in Fig. 7A. This model is consistent with previous studies suggesting N-terminal domain homology with apolipoproteins.[25, 27] Together, the N-terminal apolipophorin (left side of Fig. 7A) and C-terminal Plin3-based structural model (right side of Fig. 7A) cover all but the 18 linking residues between the two domains and the 16 C-terminal residues of Plin2, which could not be modeled due to lack of homology. A close sequence match in the PDB was found for 13 of the 18 linking residues in Plin2 (VDNAITKSELLVD) which match residues A136-A153 in PDB entry 1E6B (VNNAITKGFTALEKLLVN), formaing an alpha helix.[58] The central residues FTAL in this known structure are an insertion corresponding to a full turn of helix not found in the Plin2 sequence. Though the matching sequence comes from a glutathione S-transferase, which is unlikely to be a functional homolog of Plin2, an exact match of 9/13 residues between these two peptides means they are statistically likely to fold the same, as an alpha helix (see Table 1 in [28]). Thus, the C-terminus (yellow sphere at bottom center of Fig. 7A) of the apolipophorin-like

domain and the N-terminus (blue sphere) of the Plin3 domain may well be connected by a helical linker.

ConSurf multiple-sequence alignment of 38 diverse proteins in the Plin family yielded conservation values for each residue, which were color-mapped onto the surface of the Plin2 C-terminal domain structure and defined a cleft region (Fig. 7B). In the model, blue identified highly conserved residues with a gradient towards green, yellow, orange and red indicating decreasing chemical conservation. The Plin2 model was also colored by atom type, with blue for nitrogen atoms, green for carbon, and red for oxygen atoms (Fig. 7C). In both models the most favorable mode of stearic acid interaction with the cleft was predicted by SLIDE molecular docking[46] to reveal 5,613 favorable conformers of stearic acid generated by Omega2, including protein side-chain and ligand single-bond rotations for steric complementarity between stearic acid and Plin2. The result was an orientation of stearic acid and conformation of Plin2 side chains that yielded a favorable predicted $\Delta G_{binding}$ (-7.5 kcal/mol). The resulting orientation of stearic acid matches a highly conserved surface patch in Plin2 (blue region, Fig. 7B), as well as placing the terminal carboxylate group of stearic acid within favorable distance of conserved hydrogen-bonding groups, including the Arg236 guanidinium on helix α6, the side-chain amines of Asn329 (helix α6) and Trp398 (β4), and the main-chain nitrogen of Gly401 (β4), all absolutely conserved between Plin2 and Plin3. Since some of the deletion mutants (e.g., Plin2-N2 or Plin2-C2) remove several residues contributing to the cleft, the stearic acid binding orientation would likely differ in those cases. In fact, Plin2-C2 most likely retains lipid binding ability despite lack of key structural features of the cleft domain (helix α4, the α–β domain, and part of helix α6) due to retention of interacting residues including Asn329, Trp398 (β4), and Gly401. Docking of cholesterol into the same cleft (Fig. 7D) resulted in greater predicted affinity

of binding (-9.6 kcal/mol) relative to steric acid. Cholesterol formed interactions with several residues including Val205, Phe208, Val211, the aliphatic part of Lys213, and Tyr217 in the α-β domain, Thr325 and Val328 in helix α7, and Pro402 in strand β4. Hydrophobic contacts were also made with the collar region created by the conserved residues identified in Plin3.[25] Since these residues are conserved between Plin2 and Plin3, similar lipid interactions are also possible in Plin3.

DISCUSSION

Previous studies demonstrated that Plin2 binds lipids with high affinity[4-8] and is involved in lipid droplet formation,[1] triacylglycerol accumulation,[1-4] fatty acid uptake,[9] and lipoprotein regulation.[8, 12] Despite these findings, little is known regarding the structural and functional requirements of Plin2-lipid interactions that facilitate these processes. To address this issue, truncated Plin2 mutants were designed to contain one or more predicted domains conserved among the Plin protein family to identify structural motifs required for Plin2 lipid binding. Studies herein provide the following new insights. First, the N-terminal PAT domain is not involved in lipid binding since the Plin2-N1 mutant (containing the PAT domain) showed no evidence of binding lipids. These results are consistent with earlier studies that give evidence the PAT domain is involved in other roles including lipid droplet stabilization, lipid accumulation, and proteasomal degradation of Plin2.[24] Second, Plin2 residues 119-251, containing helix α4, the α–β domain, and part of helix α6 form a Plin3-like cleft found to be important for highest affinity lipid binding. This follows from findings that mutants containing residues 119-251 (Plin2-C1 and Plin2-N2) showed the highest affinity for cholesterol and stearic acid ligands, while those lacking these residues exhibited the least (Plin2-C2) or no (Plin2-N1) lipid binding. With Plin2-C2, NBD-stearate and NBD-cholesterol binding decreased up to 9-fold when compared to the full length protein and more than 3-fold when compared to Plin2-C1, resulting in a protein that still targeted to lipid droplets but with the lowest affinity of all the mutants that showed binding. Results finding residues 119-251 important to binding are not surprising, since the region includes structures found in the X-ray crystal of Plin3 that form a cleft of sufficient size to accommodate lipid ligands.[25] In addition, other work shows that the region of Plin2 within residues 119-426 is able to fold and function independently from the rest of the protein.[27]

Some of the residues within the cleft region however, are not entirely essential for lipid binding since removal of the α-β domain (residues 171-219) resulted in a mutant (Plin2-I) with similar binding affinity to that of the full length protein. It should also be noted affinities for the two ligands (cholesterol and stearic acid) were distinctly different. For example, Plin2-I showed a 3-fold decrease in NBD-cholesterol binding as compared to the full length protein, but with NBD-stearic acid no significant change in binding was observed. The results suggest that Plin2 has slightly different determinants for cholesterol and stearic acid binding. For instance, the proposed lipid binding site in the C-terminal domain (Fig. 7) has some shared interactions for cholesterol and stearic acid binding, but different footprints due to the different chemical structures of the individual ligands. Consistent with this, Plin2 is known to support binding to an array of lipids with diverse structures such as phospholipids, sphingomyelin, cholesterol, and fatty acids.[5-8]

Discrete targeting of the Plin2 mutants to lipid droplets was also demonstrated. Deletion mutants Plin2-N1, containing residues 1-119 (the PAT domain) and Plin2-N2, comprised of residues 1-251 (the PAT domain, helix α4, α5-β3 domain, part of helix α6) did not target to lipid droplets or show FRET interactions, consistent with earlier work demonstrating that N-terminal deletion mutants containing residues 1-131 were not found on lipid droplets.[16, 17] Addition of 52 residues to the PAT domain salvaged targeting ability in previous studies,[16, 17] suggesting the presence of a lipid droplet targeting domain in the central region of the protein. With regard to C-terminal mutants, both Plin2-C1 (containing residues 119-426) and Plin2-C2 (residues 251-426) targeted to lipid droplets, consistent with previous reports.[16, 17] However, removal of residues 154-174 in other studies[16] showed lack of targeting while exclusion of residues 172-218 in the present work resulted in a protein that targeted lipid droplets and interacted with NBD-

cholesterol in FRET assays. Despite some inconsistencies between reports, these results reinforce the idea that Plin2 contains two independent, non-overlapping targeting domains in its internal and C-terminal sequence that need consideration of the tertiary structure to understand their structure. Likewise, the fluorescence binding data supported that the ligand binding site of Plin2 is not dictated by a linear structural motif within the primary sequence. Much like the regions required for lipid droplet targeting, domains involved in forming the lipid binding pocket of the protein come from non-contiguous parts of the protein. This motivated the modeling of Plin2 tertiary structure to understand how these regions organize into functional lipid binding and targeting domains. The tertiary structure of Plin2 was modelled using Modeller and Pcons, also providing insights into the differences in ligand binding affinities among the mutant proteins. Comparative modeling revealed the Plin2 tertiary structure contained an apolipophorin III-like N-terminal domain and a TIP47-like C-terminal domain, which were linked by 18 residues. Consistent with earlier predictions and X-ray crystal data for the most similar proteins, the modeled N-terminal domain is likely to form an α-helical bundle,[26, 27] while the C-terminal domain contained a highly conserved cleft formed from the union of the α−β domain and the 4-helix bundle with high homology to the corresponding crystal structure of this region in Plin3.[25] ConSurf multiple-sequence alignment identified highly conserved residues within the Plin family which localize to the cleft. SLIDE molecular docking[46] revealed favorable conformers of stearic acid and cholesterol interaction in the cleft region. Key residues predicted to interact with stearic acid included Trp398, Gly401, and two residues in helix α6, Arg236 and Asn329 that are conserved between Plin2 and Plin3, suggesting conservation of function. Cholesterol formed interactions with several residues in the same region as stearic acid including Val205, Phe208, Val211, Lys213, and Tyr217. However, cholesterol also interacted with residues Thr325 and

Val328 in helix α7, and Pro402 in strand β4 near the C-terminal end of the protein. Orientations of stearic acid and cholesterol within the cleft were favored energetically, with cholesterol predicted to have greater affinity of binding relative to stearic acid ($\Delta G_{binding}$ of -9.6 kcal/mol versus -7.5 kcal/mol). These results were consistent with experimental binding results that showed Plin2 bound NBD-cholesterol with higher affinity than NBD-stearic acid. Deletion mutants that remove residues contributing to the cleft (e.g. Plin2-I) would also be expected to differ in binding interactions and affinity, as was observed with the experimental data demonstrating higher affinity for stearic acid than cholesterol with deletion mutant Plin2-I and decreased affinity for cholesterol when compared to the full length protein. Moreover, Plin2-C2 is missing some structures that form the cleft domain but retention of several interacting residues (Asn329, Trp398, Gly401, Thr325, Val328, and Pro402) likely contributes to its ability to bind both stearic acid and cholesterol, although at decreased affinity. Taken together, results from modeling and experiments support that the predicted cleft in the C-terminal region of Plin2 favorably binds lipids.

Finally, several trends were found in the CD, FRET, and lipid droplet targeting data. Plin2 in the absence of ligand was significantly helical. However, the percentage of helical content doubled in the Plin-C1 and Plin-C2 mutants, in which the N-terminal domain and part or all of the α-β domain were absent, suggesting that the C-terminal region is much more strongly helical than the N-terminal region. One interpretation, given the consistent sequence-based prediction of predominantly helical structure for the N-terminal half of the protein, is that the N-terminal helices are less stable and fluctuate more. These trends were preserved in the presence of both cholesterol and stearic acid, suggesting that ligand binding does not dissolve or nucleate helical structure in Plin2. Lipid droplet targeting was associated with maintenance of the helical regions

in both the N- and C-terminal helical bundles, as evidenced by Plin2 and Plin2-I being fully targeted to lipid droplets, while the other mutants were partially or fully targeted to the cytoplasm. Fluorescence binding and FRET results with labeled cholesterol support strong interactions between cholesterol and the native Plin2 structure, with weaker interactions with Plin2-C-1, Plin2-C2, Plin2-I, and Plin2-N2 constructs. No evidence for cholesterol (or stearic acid) interaction with Plin2-N1 was detected. These results support the crucial role of the C-terminal helical bundle region of Plin2 that is homologous to Plin3 (Fig. 7A, right side) for binding lipids; this region contains the conserved cleft. Other recent reports support the functional importance of the Plin family's C-terminal regions.[59, 60] The C-terminal region of Plin1 contains a C-terminal region, implicated in binding AB-hydrolase domain containing-5 (ABHD5), a cofactor that prevents the activation of adipose tissue triacylglycerol lipase. Patel *et al.*[59] demonstrated that fusing the carboxy terminal region of Plin1 to the amino terminus of Plin2 was sufficient to stabilize ABHD5 and suppress basal lipolysis. For Plin5, Sztalryd *et al.*[60] demonstrated that fusing the carboxy terminal region of Plin5 to Plin2 generated a protein that was able to recruit lipid droplets to mitochondria, whereas Plin2 by itself did not. Our work supports specific lipid binding as a function for the C-terminal region in Plin2.

In summary, the modeled tertiary structure for Plin2 highlighted the structural and functional features necessary for ligand binding and lipid droplet targeting. The PAT domain was not required for lipid binding or lipid droplet targeting; removal of this domain resulted in C-terminal mutants with high affinity for lipids. Crucial elements contained within residues 119-251 in the C-terminal region include the central α-β domain, along with the conserved end of helix α6, which form part of the cleft region. Removal of these residues decreased binding with cholesterol and stearic acid ligands several-fold. Evidence of the functional relevance of this

region was recently provided in studies with a human Plin2 variant where a serine to proline mutation at residue 251 caused individuals with the minor allele to exhibit decreased plasma triglyceride and decreased VLDL levels.[12] Structurally, the mutation would be predicted to disrupt helix α6. In the present work, both cholesterol and stearic acid were shown through molecular docking experiments to interact favorably with a cleft formed by conserved residues within the C-terminal region, including helix α6. Furthermore, the modeled interactions together with the mutant construct binding studies suggest that this conserved cleft is a site of favorable lipid interaction for both cholesterol and stearic acid.

Acknowledgements. We would like to thank Ken Moon for his technical assistance. We thank OpenEye Scientific Software (Santa Fe, NM) for providing academic licenses for their Omega2 and QUACPAC (Molcharge) software.

REFERENCES

1. Fukushima, M., Enjoji, M., Kohjima, M., Sugimoto, R., Ohta, S., Kotoh, K., Kuniyoshi, M., Kobayashi, K., Imamura, M., Inoguchi, T., Nakamuta, M., and Nawata, H. (2005) Adipose differentiation related protein induces lipid accumulation and lipid droplet formation in hepatic stellate cells, *In Vitro Cell Dev Biol Anim 41*, 321-324.
2. Larigauderie, G., Cuaz-Perolin, C., Younes, A. B., Furman, C., Lasselin, C., Copin, C., Jaye, M., Fuchart, J. C., and Rouis, M. (2006) Adipophilin increases triglyceride storage in human macrophages by simulation of biosynthesis and inhibition of beta-oxidation, *FEBS J 273*, 3498-3510.
3. Listenberger, L. L., Ostermeyer-Fay, A. G., Goldberg, E. B., Brown, W. J., and Brown, D. A. (2007) Adipocyte differentiation-related protein reduces the lipid droplet association of adipose triglyceride lipase and slows triacyglycerol turnover, *J Lipid Res 48*, 2751-2761.
4. McIntosh AL, Senthivinayagam S, Moon KC, Gupta S, Lwande JS, Murphy CC, Storey S, and Atshaves BP. (2012) Direct interaction of ADRP with lipids on the surface of lipid droplets: A live cell FRET analysis., *Am J Physiol Cell Physiol 303*, C728-742.
5. Serrero, G., Frolov, A., Schroeder, F., Tanaka, K., and Gelhaar, L. (2000) Adipose differentiation related protein. Expression, purification of recombinant protein in E. coli and characterization of its fatty acid binding properties, *Biochim Biophys Acta 1488*, 245-254.
6. Atshaves, B. P., Storey, S. M., McIntosh, A. L., Peterscu, A. D., Lyuksyutova, O. I., Greenberg, A. S., and Schroeder, F. (2001) Sterol carrier protein 2 expression modulates

protein and lipid composition of lipid droplets, *J Biol Chem 276*, 25324-25335.

7. McIntosh, A. L., Storey, S. M., and Atshaves, B. P. (2010) Intracellular lipid droplets contain dynamic pools of sphingomyelin: ADRP binds phopholipids with high affinity, *Lipids 45*, 465-477.

8. Frolov, A., Petrescu, A., Atshaves, B. P., So, P. T. C., Gratton, E., Serrero, G., and Schroeder, F. (2000) High density lipoprotein mediated cholesterol uptake and targeting to lipid droplets in intact L-cell fibroblasts, *J Biol Chem 275*, 12769-12780. .

9. Gao, J., and Serrero, G. (1999) Adipose differentiation related protein (ADRP) expressed in transfected COS-7 cells selectively stimulates long chain fatty acid uptake, *J Biol Chem 274*, 16825-16830.

10. Atshaves, B. P., Starodub, O., McIntosh, A. L., Roths, J. B., Kier, A. B., and Schroeder, F. (2000) Sterol carrier protein-2 alters HDL-mediated cholesterol efflux, *J Biol Chem 275*, 36852-36861.

11. Chang, B. H., Li, L., Saha, P., and Chan, L. (2010) Absence of adipose differentiation related protein upregulates hepatic VLDL secretion, relieves hepatosteatosis, and improves whole body insulin resistance in leptin-deficient mice, *J Lipid Res 51*, 2132-2142.

12. Magne, J., Aminoff, A., Sundelin, J., Mannila, M. N., Gustafsson, P., Hultenby, K., Wernerson, A., Bauer, G., Listenberger, L. L., Neville, M., Karpe, F., Boren, J., and Ehrenborg, E. (2013) The minor allele of the missense polymorphism Ser251Pro in perilipin 2 (PLIN2) disrupts an α-helix, affect lipolysis, and is associated with reduced plasma tryglyceride concentration in humans, *FASEB J 27*, 3090-3099.

13. Brasaemle, D. L., Subramanian, V., Garcia, A., Marcinkiewicz, A., and Rothenberg, A.

(2009) Perilipin A and the control of triacylglycerol metabolism, *Mol Cell Biochem 326*, 15-21.

14. Subramanian, V., Garcia, A., Sekowski, A., and Brasaemle, D. L. (2004) Hydrophobic sequences target and anchor perilipin A to lipid droplets., *J Lipid Res 45*, 1983-1991.

15. Fujimoto, T., Kogo, H., Ishiguro, K., Tauchi, K., and Nomura, R. (2001) Caveolin-2 is targeted to lipid droplets, a new membrane domain in the cell, *J.Cell.Biol. 152*, 1079-1085.

16. Nakamura, N., and Fujimoto, T. (2003) Adipose differentiation-related protein has two independent domains for targeting to lipid droplets, *Biochem Biophys Res Comm 306*, 333-338.

17. Targett-Adams, P., Chambers, D., Gledhill, S., Hope, R. G., Coy, J. F., Girod, A., and McLauchlan, J. (2003) Live cell analysis and targeting of the lipid droplet-binding adipocyte differentiation-related protein, *J Biol Chem 278*, 15998-16007.

18. Wiener, M. (2005) A census of ordered lipids and detergents in X-ray crystal structures of integral membrane proteins, In *Protein-Lipid Interactions: From Membrane Domains to Cellular Networks* (Tamm, L., Ed.), Wiley-VCH Verlag GmbH & Co, New York.

19. Qin, L., Sharpe, M., Garavito, R., and Ferguson-Miller, S. (2007) Conserved lipid-binding sites in membrane proteins: a focus on cytochrome c oxidase, *Current Opinion in Structural Biology 17*, 444-450.

20. Hanson, M., Cherezov, V., Roth, C., Griffith, M., Jaakola, V.-P., Chien, E., Valasquez, J., Kuhn, P., and Stevens, R. (2008) A specifc cholesterol binding site is established by the 2.8 A structure of human β_2-adrenergic receptor in an alternate crystal form., *Structure 16*, 897-905.

21. Adamian, L., Naveed, H., and Liang, J. (2011) Lipid-binding surfaces of membrane proteins:Evidence from evolutionary and structural analysis, *Biochem Biophys Acta 1808*, 1092-1102.

22. Garcia, A., Sekowski, A., Subramanian, V., and Brasaemle, D. (2003) The central domain is required to target and anchor Perilipin A to lipid droplets, *J Biol Chem 278*, 625-635.

23. Miura, S., Gan, J. w., Brzostowski, J., Parisi, M. J., Schultz, C. J., Londos, C., Oliver, B., and Kimmel, A. R. (2002) Functional conservation for lipid storage droplet association among perilipin, ADRP, and TIP47 (PAT)-related proteins in mammals, Drosophila, and dictyostelium, *J Biol Chem 277*, 32253-32257.

24. Orlicky, D. J., DeGala, G., Greenwood, C., Bales, E. S., Russell, T. D., and McManaman, J. L. (2008) Multiple function encoded by the N-terminal PAT domain of adipophilin, *J Cell Science 121*, 2921-2929.

25. Hickenbottom, S. J., Kimmel, A. R., Londos, C., and Hurley, J. H. (2004) Structure of a lipid droplet protein: The PAT family member TIP47, *Structure 12*, 1199-1207.

26. McManaman, J. L., Zabaronick, W., Schaack, J., and Orlicky, D. J. (2003) Lipid droplet targeting domains of adipophilin, *J Lipid Res 44*, 668-673.

27. Chong, B. M., Russell, T. D., Schaack, J., Orlicky, D. J., Reigan, P., Ladinsky, M., and McManaman, J. L. (2011) The adipophilin C terminus is a self-folding membrane binding domain that is important for milk lipid secretion, *J Biol Chem 286*, 23254-23265.

28. Sander, C., and Schneider, R. (1991) Database of homology-derived protein structure and the structureal meaning of sequence alignment., *Protein: Structure, Function, and Genetics 9*, 56-68.

29. Chong, B. M., Reigan, P., Mayle-Combs, K. D., Orlicky, D. J., and McManaman, J. L. (2011) Determinants of adipophilin function in milk lipid formation and secretion, *Trends Endocrin Metab 22*, 211-217.

30. Bussell, R., and Eliezer, D. (2003) A strucutral and functional role for 11-mer repeats in alpha-synuclein and other exchangeable lipid binding proteins., *J Mol Biol 329*, 763-778.

31. Atshaves, B. P., Petrescu, A. D., Starodub, O., Roths, J. B., Kier, A. B., and Schroeder, F. (1999) Expression and intracellular processing of the 58 KDa SCP-x/3-oxoacyl-CoA thiolase in transfected mouse L cells, *J Lipid Res 40*, 610-622.

32. Hansson, M. D., Rzeznicka, K., Rosenback, M., Hansson, M., and Sirijovski, N. (2008) PCR-mediated deletion of plasmid DNA., *Anal Biochem 375*, 373-375.

33. Hopp, T. P., and Woods, K. R. (1981) Prediction of protein antigenic determinants from amino acid sequences., *Proc Natl Acad Sci USA 78*, 3824.

34. Rost, B., and Sander, C. (1994) Combing evolutionary information and neural networks to predict protein secondary structure., *Proteins 19*, 55-72.

35. Jones, D. T. (1999) Protein secondary structure prediction basedo on position-specific scoring matrices., *J Mol Biol 292*, 195-202.

36. McGuffin, L. J., Bryson, K., and Jones, D. T. (2000) The PSIPRED protein structure prediction server, *Bioinformatics 16*, 404-405.

37. Karplus, K., Karchin, R., Barrett, C., Tu, S., Cline, M., Diekhans, M., Grate, L., Casper, J., and Hughey, R. (2001) What is the value added by human intervention in protein structure prediction?, *Proteins: Struct Funct Genet Suppl 5*, 86-91.

38. Adamczak, R., Porollo, A., and Meller, J. (2005) Combining prediction of secondary structure and solvent accessibility in proteins., *Proteins: Struct Funct Genet 59*, 467-475.

39. Bernstein, F., Koetzle, T., Williams, G., Meyer, E., Brice, M., Rodgers, J., Kennard, O., Shimanouchi, T., and Tasumi, M. (1977) The protein data bank: A computer-based archival file for macromolecular structures., *Eur J Biochem 80*, 319-324.

40. Marti-Renom, M. A., Stuart, A., Fiser, A., Sanchez, R., Melo, F., and Sali, A. (2000) Comparative protein structure modeling of genes and genomes, *Annu Rev Biophys Biomol Struct 29*, 291-325.

41. Eswar, N., Mari-Renom, M. A., Webb, B., Madhusudhan, M. S., Eramian, D., Shen, M., Pieper, U., and Sali, A. (2006) Comparative protein structure modeling with MODELLER, *Curr Protocols Bioinform Supl 15*, 5.6.1-5.6.30.

42. Landau, M., Mayrose, I., Rosenberg, Y., Glaser, F., Martz, E., Pupko, T., and Ben-Tal, N. (2005) Con/Surf 2005: The projection of evolutionary conservation scores of residues on protein structures., *Nucleic Acids Res. 33*.

43. Glaser, F., Pupko, T., Paz, I., Bell, R. E., Bechor, D., Martz, E., and Ben-Tal, N. (2003) ConSurf: Identification of functional regions in proteins by surface-mapping of phylogenetic information., *Bioinformatics 19*, 163-164.

44. Young, A., Scapin, G., Kromminga, A., Patel, S., Veerkamp, J., and Sacchettini, J. (1994) Structural studies on human muscle fatty acid binding at 1.4 A resolution: binding interactions with three C18 fatty acids., *Structure 2*, 523-534.

45. Morth, J., Pedersen, P., Toustrup-Jensen, M., Sorensen, T., Petersen, J., Andersen, J., Vilsen, B., and Nissen, P. (2007) Crystal structure of the sodium-potassium pump., *Nature 450*, 1043-1049.

46. Zavodszky, M. I., Sanschagrin, P. C., Korde, R. S., and Kuhn, L. A. (2002) Distilling the essential features of a protein surface for improving protein-ligand docking, scoring and

virtual screening., *J Comp-aided Mol Design 16*, 883-902.

47. Thumser, A. E. A., and Wilton, D. C. (1994) Characterization of binding and structural properties of rat liver fatty-acid-binding protein using tryptophan mutants, *Biochem J 300*, 827-833.

48. Rawel, H., Frey, S., Meidtner, K., Kroll, J., and Schweigert, F. (2006) Determining the binding affinities of phenolic compounds to proteins by quenching of the intrinsic tryptophan fluorescence, *Mol Nutr Food Res 50*, 705-713.

49. Hostetler, H., Kier, A., and Schroeder, F. (2006) Very-long-chain and branched-chain fatty acyl-CoAs are high affinity ligands for the peroxisome proliferatror-activated receptor α (PPARα), *Biochemistry 45*, 7669-7681.

50. Senthivinayagam, S., McIntosh, A. L., Moon, K. C., and Atshaves, B. P. (2013) Plin2 inhibitis cellular glucose uptake through interactions with SNAP23, a SNARE complex protein, *PLoS ONE 8*, e73696. doi: 73610.71371/journal.pone.0073696.

51. Sreerama, N., and Woody, R. W. (2000) Estimation of protein secondary structure from circular dichroism spectra: comparison of CONTIN, SELCON, and CDSSTR methods with an expanded reference set, *Anal Biochem 287*, 252-260.

52. Lakowicz, J. (1999) *Principles of Fluorescence Spectroscopy*, Kluwer Academic/Plenum Publishers, New York.

53. Teale, F., and Weber, G. (1957) Ultraviolet flurescence of the aromatic amino acids, *Biochem J 65*, 476-482.

54. Frolov, A., and Schroeder, F. (1998) Acyl coenzyme A binding protein. Conformational sensitivity to long chain fatty acyl-CoA, *J Biol Chem 273*, 11049-11055.

55. Frolov, A., and Schroeder, F. (1998) Acyl Coenyme A Binding Protein, *The Journal of*

Biological Chemistry 273, 11049-11055.

56. Breiter, D. R., Kanost, M. R., Benning, M. M., Wesenberg, G., Law, J. H., Wells, M. A., Rayment, I., and Holden, H. M. (1991) Molecular structure of an apolipoprotein determined at 2.5-A resolution, *Biochemistry 30*, 603.

57. Ajees, A. A., Anantharamaiah, G. M., Mishra, V. K., Hussain, M. M., and Murthy, K. H. M. (2006) Crystal structure of human apolipoprotein A-I: Insights into its protective effect against cardiovascular diseases., *Proc Natl Acad Sci USA 103*, 2126.

58. Dixon, T., Edwards, D., Cole, D., and Lapthorn, A. (2001) The structure of a zeta class glutathione S-transferase from Arabidopsis thaliana: characterisation of a GST with novel active-site architecture and a putative role in tyrosine catabolism., *J Mol Biol 308*, 949-962.

59. Patel, S., Yang, W., Kozusko, K., Saudek, V., and Savage, D. (2014) Perilipins 2 and 3 lack a carboxy-terminal domain present in perilipin1 involved in sequestering ABHD5 and supressing basal lipolysis, *Proc Natl Acad Sci USA 111*, 9163-9168.

60. Wang, H., Sreenevasan, U., Hu, H., Saladino, A., Polster, B. M., Lund, L. M., Gong, D. W., Stanley, W. A., and Sztalryd, C. (2011) Perilipin 5, a lipid droplet-associated protein, provides physical and metabolic linkage to mitochondria, *J Lipid Res 52*, 2159-2168.

Table 1. Cholesterol and stearic acid binding to Plin2 and the deletion mutants.

	NBD-Cholesterol		NBD-Stearic Acid	
Protein	K_d (nM)	λmax (nm)	K_d (nM)	λmax (nm)
Plin2	11 ± 2	543	121 ± 12	544
Plin2-C1	48 ± 3*,@	540	69 ± 7*,@	538
Plin2-C2	98 ± 10*	545	160 ± 3*	544
Plin2-N1	ND	548	ND	545
Plin2-N2	50 ± 6*,@	543	92 ± 14@	547
Plin2-I	34 ± 4*,@	540	90 ± 7@	540

The dissociation constant (K_d) and emission maximum (λmax) of Plin2 and the deletion mutants for NBD-labeled cholesterol and stearic acid were determined using a fluorescent lipid binding assay as described in the Methods section. Values represent the mean ± SE (n=3-4). (*) indicates $P \leq 0.05$ as compared to full length Plin2. (@) indicates $P \leq 0.05$ as compared to Plin2-C2. ND indicates no detectable binding was observed.

Table 2. Intracellular targeting and FRET analysis of Plin2 and the deletion mutants in transfected L cells.

Protein	Intracellular Targeting	*E* (%)	*R* (Å)
Plin2	LD	25 ± 5	77 ± 4
Plin2-C1	LD, Cytosol	7 ± 1	96 ± 4
Plin2-C2	LD, Cytosol	13 ± 3	85 ± 4
Plin2-N1	Cytosol	ND	ND
Plin2-N2	LD, Cytosol	ND	ND
Plin2-I	LD	9 ± 1	92 ± 3

Intracellular targeting, FRET efficiencies *E*, and distance *R* between Cy5-labeled Plin2 deletion proteins and NBD-cholesterol were determined as described in the Experimental section. FRET was not detected (ND) in Plin2-N1 or Plin2-N2 expression cells. Values reflect mean ± SE from $n \geq 20$ lipid droplets (LD) from 20-30 cells. Intracellular targeting indicated localization sites of Cy5-Plin2 (red) and NBD-Cholesterol (green) where yellow-to-orange indicated colocalization of the probes.

Table 3. Predicted secondary structures of Plin2 and the deletion mutants in the presence and absence of cholesterol and stearic acid.

		Secondary Structure (%)					
		H(r)	H(d)	S(r)	S(d)	Turns	Unrd
Plin2	(-)Ligand	10.3±0.1	11.5±0.2	15.0±0.1	9.5±0.1	21.8±0.1	31.7±0.1
	(+)Chol	12.05±0.4**	11.7±0.3	15.3±0.1	9.4±0.1	21.5±0.4	31.1±0.2
	(+)SA	9.9±0.1**	11.1±0.2	15.0±0.3	9.9±0.1**	21.9±0.1	32.2±0.2
Plin2-C1	(-)Ligand	21.3±0.2*	19.6±0.6*	6.1±0.6*	5.4±0.4*	19.1±1	28.0±0.5*
	(+)Chol	27.7±0.2**	23.6±0.2**	5.0±0.1	4.9±0.1	18.2±0.2	26.9±0.2
	(+)SA	18.3±0.2**	18.3±0.2	7.0±0.6	6.5±0.1	20.9±0.8	29.2±0.4
Plin2-C2	(-)Ligand	18.6±0.1*	14.2 ± 0.1*	11.2±0.1*	7.9±0.1*	19.1±0.1*	29.1±0.1*
	(+)Chol	19.6±0.4	13.4±0.1**	11.3±0.7	8.1±0.1	19.1±0.5	29.7±0.2
	(+)SA	18.8±0.1	14.1±0.1	11.3±0.1	8.0±0.1	19.0±0.2	28.6±0.1**
Plin2-I	(-)Ligand	7.5±0.2*	8.9±0.1*	19.0±0.2*	11.2±0.1*	21.9±0.1	30.6±0.1*
	(+)Chol	6.3±0.1**	9.1±0.1	19.4±0.1	11.2±0.1	21.8±0.1	30.9±0.2
	(+)SA	6.9±0.1	8.5±0.1**	19.9±0.1**	11.6±0.1**	22.1±0.1	30.3±0.1
Plin2-N1	(-)Ligand	0.8±0.5*	2.5±0.8*	26±3*	14±1*	27±2	30±4
	(+)Chol	0.4±0.1	3.8±0.2	26.5±0.7	12.5±0.1	22.1±0.6	33.8±0.2
	(+)SA	0.1±0.1	3.6±0.4	25.7±0.2	12.4±0.1	24±1	32±1
Plin2-N2	(-)Ligand	6.5±0.1*	10.0±0.2*	16.5±0.1*	10.7±0.1*	23.4±0.1*	33.0±0.2*
	(+)Chol	5.2±0.4**	7.1±0.4**	18.1±0.3**	11.0±0.2	23±1	33±1
	(+)SA	6.9±0.2	10.4±0.1	16.1±0.1**	10.6±0.1	23.5±0.2	32.6±0.2

All conditions were as described in the Methods section. Values represent the mean ± SE (10 iterations/run performed in triplicate) analyzed by CDSSTR. H(r) indicates regular α-helices; H(d), distorted α-helices; S(r), regular β-sheets; S(d), distorted β-sheets; Unrd, unordered structures. Chol refers to cholesterol and SA to stearic acid. (*) indicates $P \leq 0.05$ as compared to Plin2 without ligand. (**) indicates $P \leq 0.05$ as compared to each protein in the absence of ligand.

FIGURE LEGENDS

Figure 1. Predicted secondary structure and conserved domains of Plin2. Based on prediction software (SABLE2, SAM and PsiPRED) and the known X-ray crystal structure of the homologous Plin3 protein, the predicted structure of Plin2 (A) contains 9 α-helices and 5 small β strands inter-connected by random coils and unordered structure. Several regions of interest include the PAT domain (B), 11-mer repeat region (A), two lipid droplet (LD) targeting domains (B), and the C-terminal area containing an α–β domain (A) and 4 Helix bundle (A) that together formed a cleft region. Residues that line the cleft (indicated by *) include: Val-203, Tyr-215, Ala-233, Arg-236, Val-237, Ala-240, Thr-325, Val-326, Asn-329, Gln-331, Trp-398, Leu-399, Val-400, Pro-402 and Phe-403. Hopp-Woods hydrophilicity plots for Plin2 (C) and Plin3 (D) were generated using a server at the Colorado State University (http://www.vivo.colostate.edu/molkit/hydropathy/index.html) to provide predicted hydrophilic (lines above zero) and hydrophobic regions (below zero) within the proteins. Line diagrams of Plin2 and the deletion mutants (E) include full length Plin2 (containing amino acid residues 1-425); Plin2-C1 (residues 119-425); Plin2-C2 (residues 251-425); Plin2-N1 (residues 1-119); and Plin2-N2 (residues 1-251); and Plin2-I (residues1-171 and 219-425).

Figure 2. Urea denaturation and circular dichroism of Plin2 as a function of temperature. Protein-denaturation studies were performed by addition of increasing aliquots of urea (0-6.0M) to recombinant Plin2. The tryptophan emission spectra (A) upon excitation at 280 nm and percent fluorescence of initial (B) was determined to show the overall effect of solvent polarity upon protein stability. Exposure of tryptophan residues to solvent upon denaturation resulted in decreased fluorescence due to quenching of residues. The effect of temperature on Plin2 secondary structure was determined by circular dichroism (C) to show Plin2 unfolding at

temperatures above 40^0C.

Figure 3. Tryptophan quenching binding assays. The Plin2 binding affinity for cholesterol (A) and stearic acid (B) was determined when titered with increasing amounts of ligand (1-120 nM) using a quenching of tryptophan fluorescence assay as described in the Experimental section. Inset, a linear plot of 1/(1–F/Fmax) versus [ligand]/(F/Fmax) allowed determination of the dissociation constant K_d where the slope of the line = 1/ K_d and the ordinate intercept = nE_o/ K_d and F represented fluorescence intensity at a given concentration of ligand, Fmax was the maximal fluorescence, [ligand] was the ligand concentration, E_o was the protein concentration, and n equaled the number of binding sites. Analysis of multiple curves yielded $K_d = 7 \pm 1$ nM and 80 ± 9 nM for cholesterol and stearic acid, respectively.

Figure 4. Titration of Plin2 and the deletion mutant proteins with NBD-Cholesterol. The binding affinities of Plin2 (A), Plin2-C1 (B), Plin2-C2 (C), Plin2-N1 (D), Plin2-N2 (E), Plin2-I (F), and non-cholesterol binding protein ACBP (G) for NBD-Cholesterol were determined using a fluorescence binding assay. The titration of the recombinant proteins with NBD-Cholesterol was followed by an increase in fluorescence (excitation 480 nm, emission 540 nm). The data representing the mean $\pm$ SE of three independent measurements was fit to a single binding site model as described in the Experimental section. Inset, a linear plot of 1/(1–F/Fmax) versus [ligand]/(F/Fmax) was used to determine the K_d as previously described where F represented fluorescence intensity at a given concentration of ligand, Fmax was the maximal fluorescence, and [ligand] was the ligand concentration.

Figure 5. Confocal microscopy colocalization of NBD-Cholesterol and Cy5-labeled cells expressing Plin2 and the deletion mutants. Colocalization experiments of NBD-Cholesterol and Cy5-labeled L cells overexpressing Plin2 (A), Plin2-C1 (B), Plin2-C2 (C), Plin2-N1 (D), Plin2-

N2 (E), or Plin2-I (F) were performed as described in the Methods section. Images were acquired sequentially and fluorescence emission was detected upon 488 nm excitation and 500/100 band path emission filter for NBD-Cholesterol (green channel) and 635 nm excitation with a 725/30 band path filter for the Cy5 emission (red channel). Images derived from the red and green channels were combined and appeared as yellow to orange where superimposition of images derived from the red and green channels overlapped.

Figure 6. Circular dichroic analysis of Plin2 and the deletion mutants. Far ultraviolet (UV) circular dichroic (CD) spectra of Plin2 (A), Plin2-C1 (B), Plin2-C2 (C), Plin2-N1 (D), Plin2-N2 (E), and Plin2-I (F) was shown in the presence or absence of ligand (cholesterol or stearic acid). Solid line indicates protein without ligand. Spectral trace designated by closed circles indicates protein incubated with cholesterol; open circle indicates protein incubated with stearic acid. Each spectrum represents an average of ten scans repeated in triplicate.

Figure 7. Plin2 has an apophorin-like N-terminal domain and a Plin3-like C-terminal domain containing a potential lipid binding cleft. The N-terminal domain structure of Plin2 (residues 1-171; shown in yellow ribbons) was modeled using the nfold fold recognition server via Pcons, based on the high degree of Plin2 sequence and secondary structural compatibility with the 3-dimensional structure of apolipophorin III (PDB entry 1AEP) and this model's consensus with the top-scoring results from 11 other fold recognition predictions for the N-terminal Plin2 sequence, all of which are alpha-helical bundles. This structure contains 5 helices connected by turns in a compact bundle. This model for the N-terminal 171 residues of Plin2 received a Pcons consensus score of 0.77, indicating a high degree of shared features with the top-scoring models from the different fold recognition methods. A value of 0.77 corresponds to 98% sensitivity

(meaning 98% of the proteins of similar fold are predicted correctly) and 94% specificity (meaning that 94% of proteins with dissimilar folds will not be incorrectly assigned as similar in fold). The homology model of the C-terminal domain of Plin2 appears to the right in panel (A), based on its 38% sequence identity with the crystal structure of the corresponding region in Plin3 (residues 191-437, PDB entry 1SZI). The structure contains a 4-helix bundle (cyan, green, orange and red helices), which together with an α-β domain (blue, magenta and light grey) form the cleft. Stearic acid (the U-shaped light blue-colored stick figure, with carboxylate oxygens in red) is shown positioned in this cleft, based on the most energetically favorable binding mode predicted by SLIDE.[46] Cleft residues include Val203, Tyr215, Ala233, Arg236, Val237, Ala240, Thr325, Val326, Asn329, Gln331, Trp398, Leu399, Val400, Pro402 and Phe403. (B) ConSurf analysis of residue conservation in the perilipin family, color-mapped onto the surface of the Plin2 C-terminal domain. The position of the cleft is indicated by the predicted binding mode for stearic acid (light blue stick figure). Dark blue to green surface indicates the most highly and next most highly conserved residues in perilipins mapped onto the Plin2 structure, and yellow to red indicate increasingly low conservation. (C) Atom-colored surface representation of the same region in Plin2 (green for carbon, blue for nitrogen, and red for oxygen atoms). Hydrogen-bonding atoms are found deep in the cleft ringed by hydrophobic surface, positioned such that they can bridge to the predicted position of the carboxylate group in stearic acid. (D) Predicted most favorable mode of cholesterol binding (pink tubes) with the conserved cleft of Plin2, shown with surface colored by residue conservation (as in panel B, above).

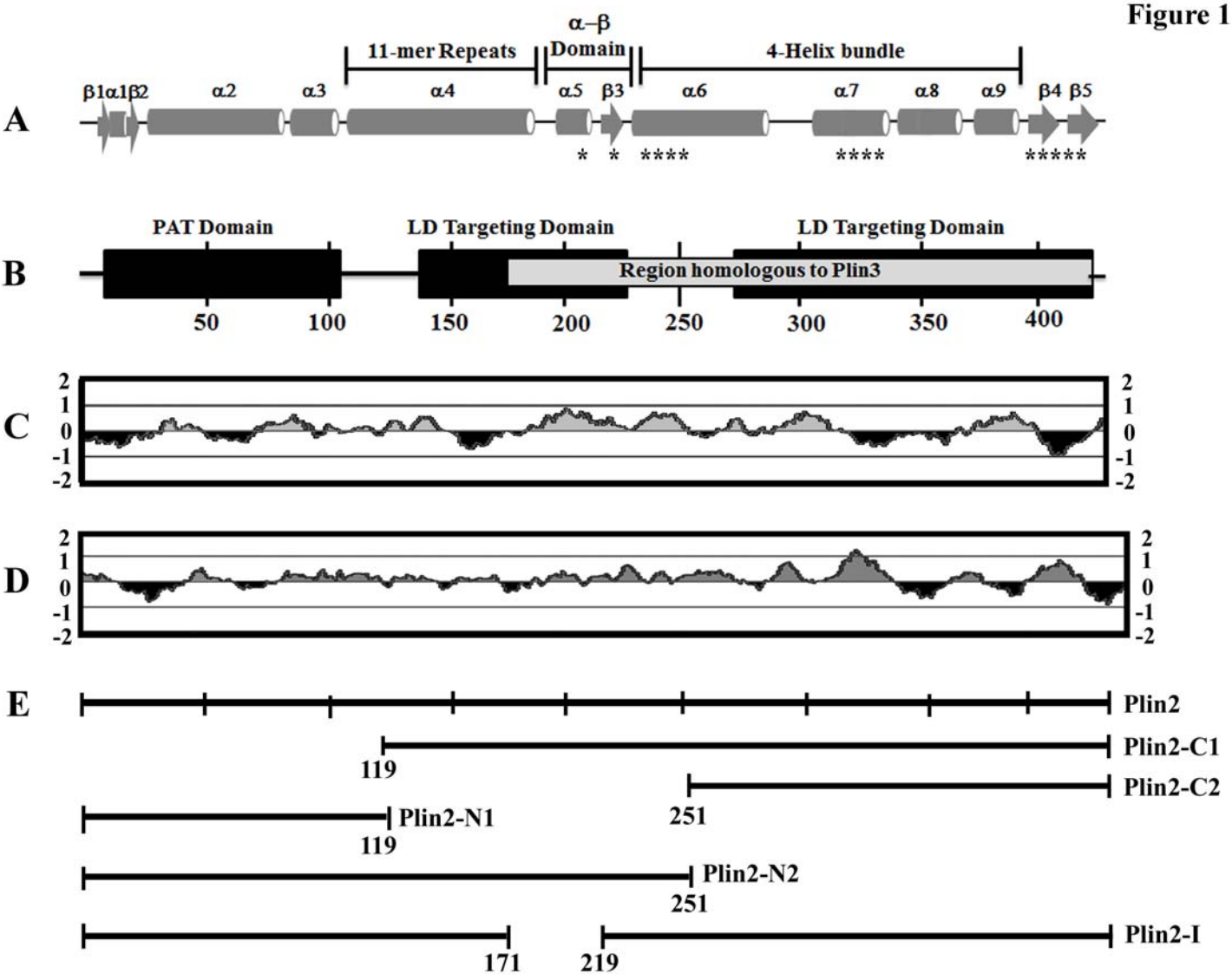
α–β
Domain
11-mer Repeats
4-Helix bundle
A
β1α1β2
α2
α3
α4
α5
β3
α6
α7
α8
α9
β4 β5
PAT Domain
LD Targeting Domain
LD Targeting Domain
B
Region homologous to Plin3
50
100
150
200
250
300
350
400
C
D
E
Plin2
Plin2-C1
119
Plin2-C2
251
Plin2-N1
119
Plin2-N2
251
Plin2-I
171
219

Figure 1

Figure 2

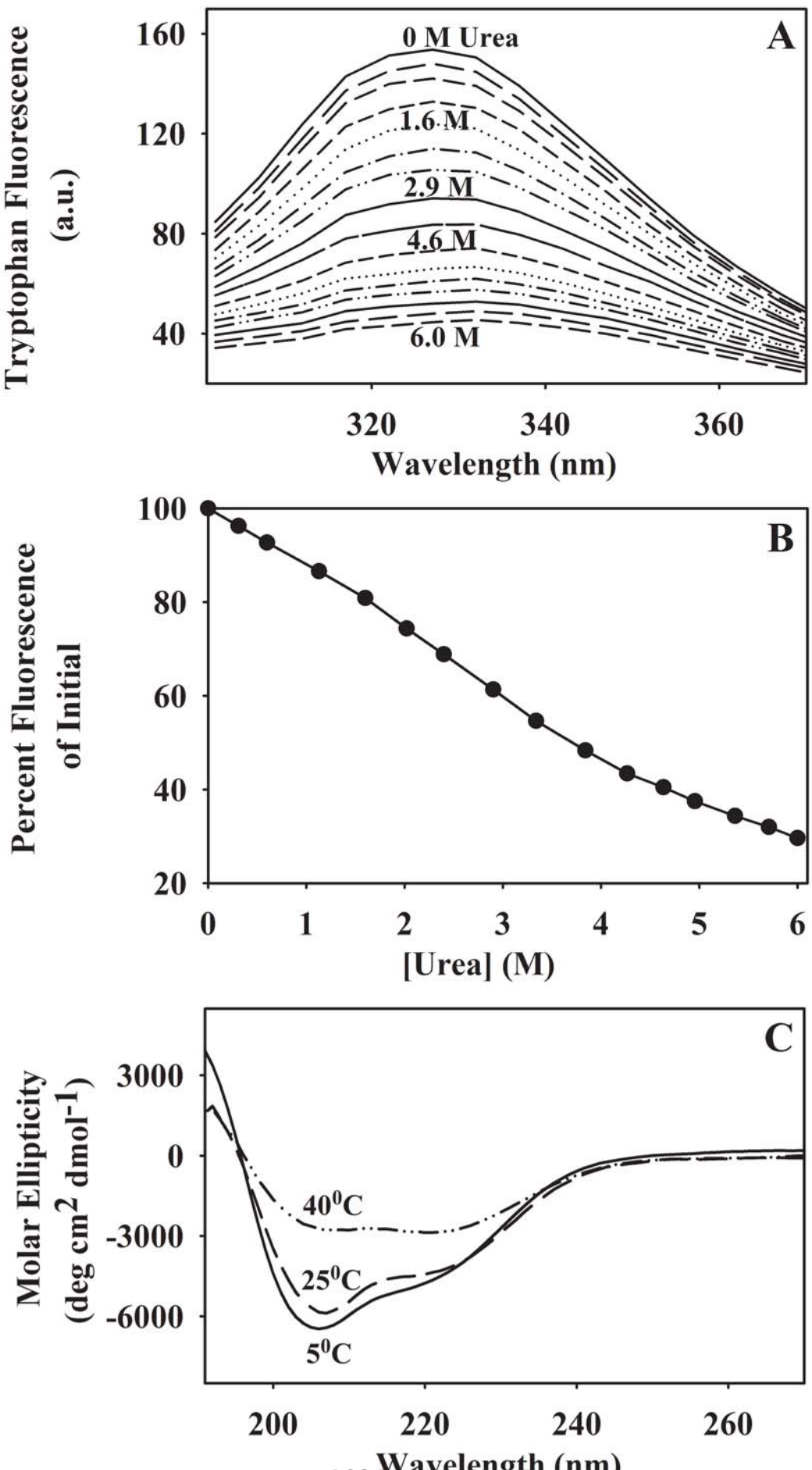

Figure 3

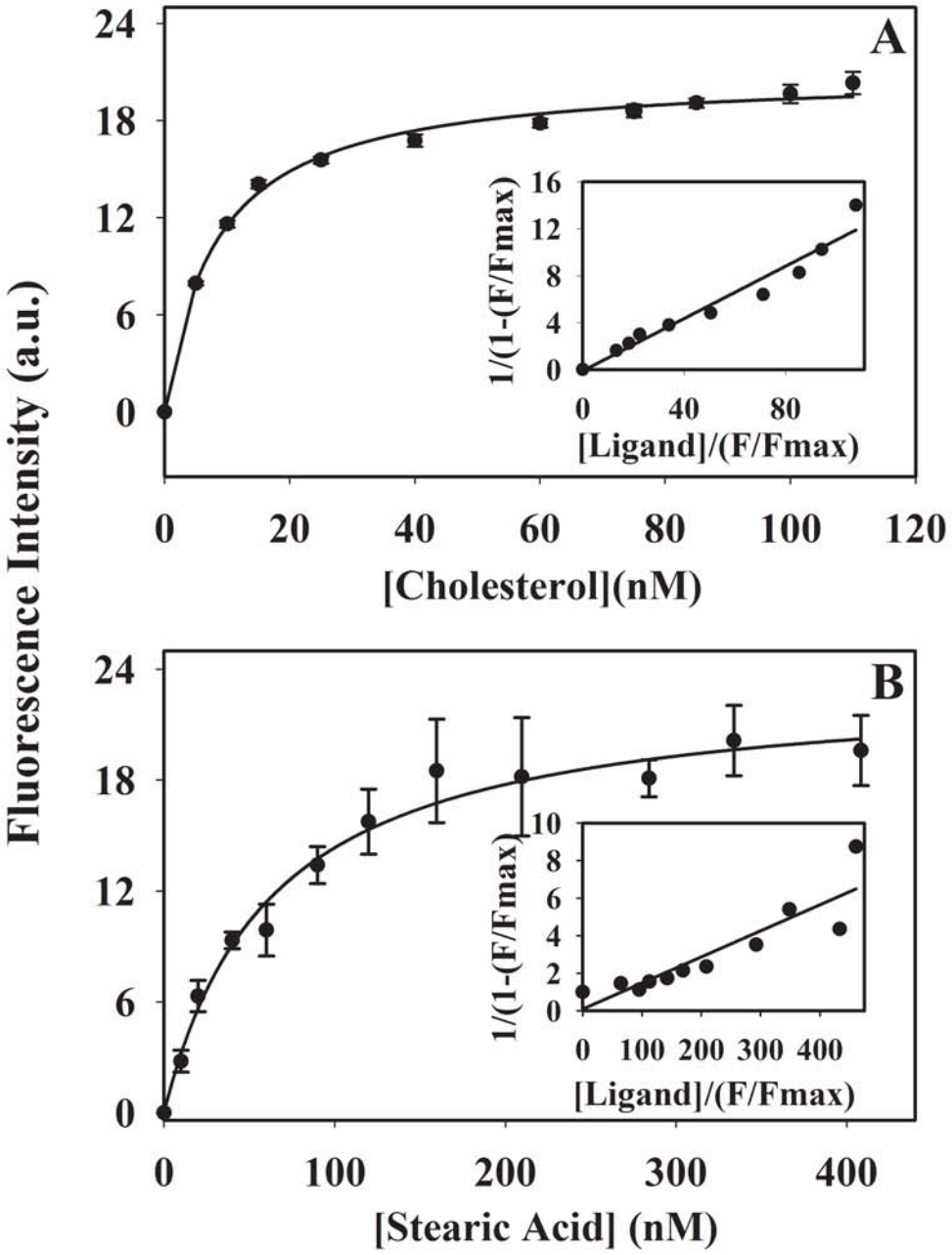
A
Fluorescence Intensity (a.u.)
[Cholesterol](nM)
1/(1-(F/Fmax)
[Ligand]/(F/Fmax)
B
[Stearic Acid] (nM)

Figure 4

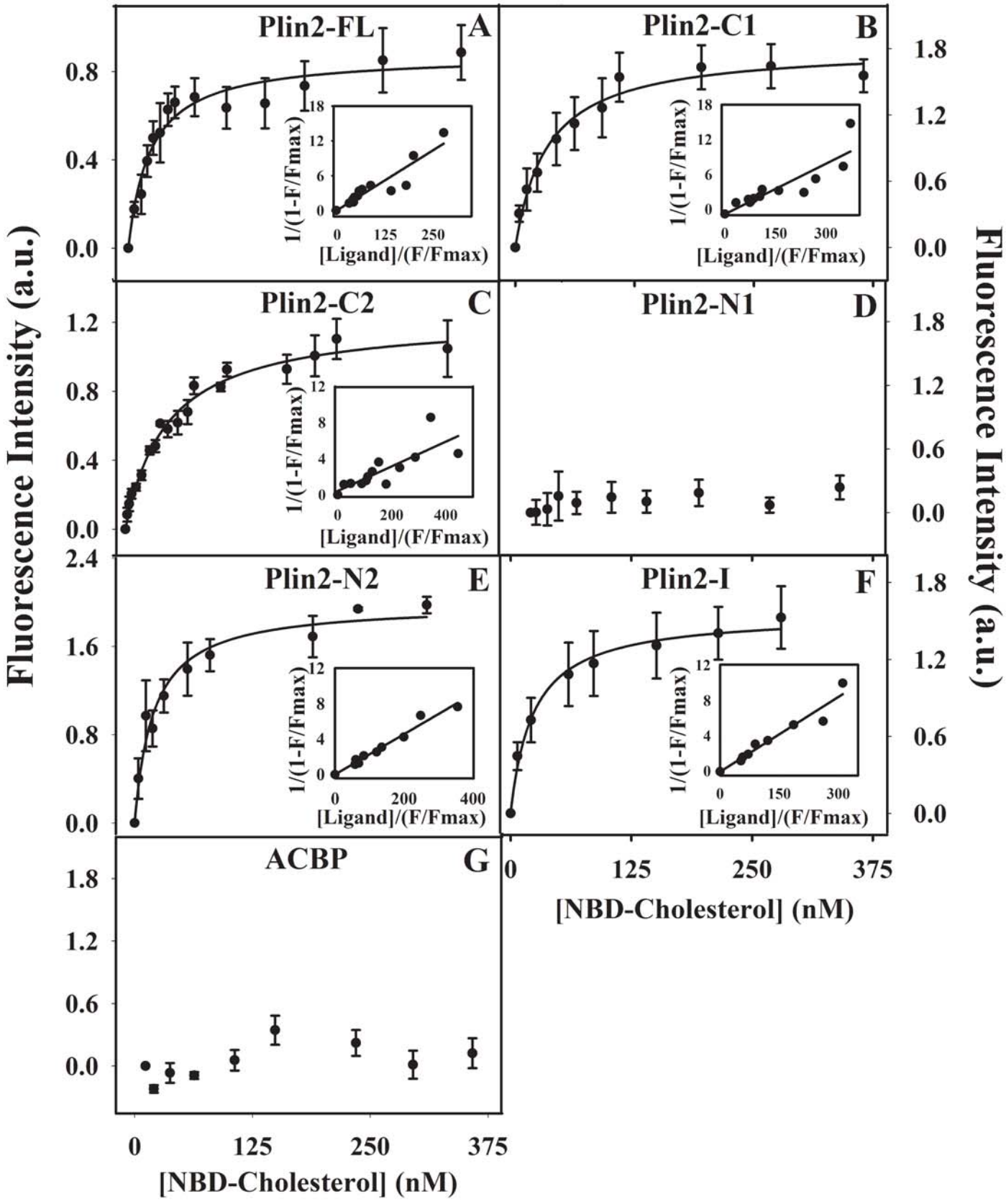
Plin2-FL
A
Plin2-C1
B
Plin2-C2
C
Plin2-N1
D
Plin2-N2
E
Plin2-I
F
ACBP
G
1/(1-F/Fmax)
[Ligand]/(F/Fmax)
Fluorescence Intensity (a.u.)
[NBD-Cholesterol] (nM)

Figure 5

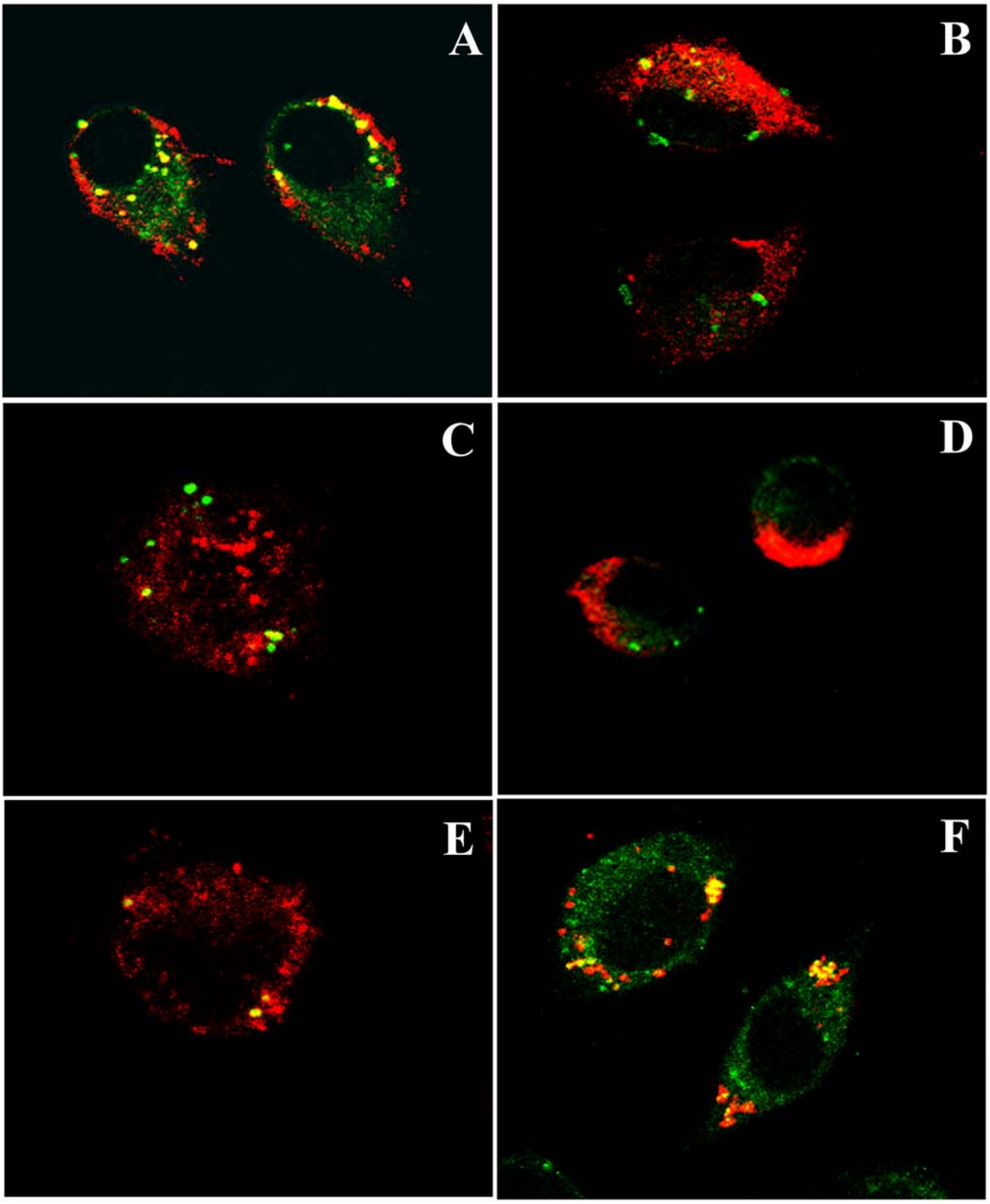

Figure 6

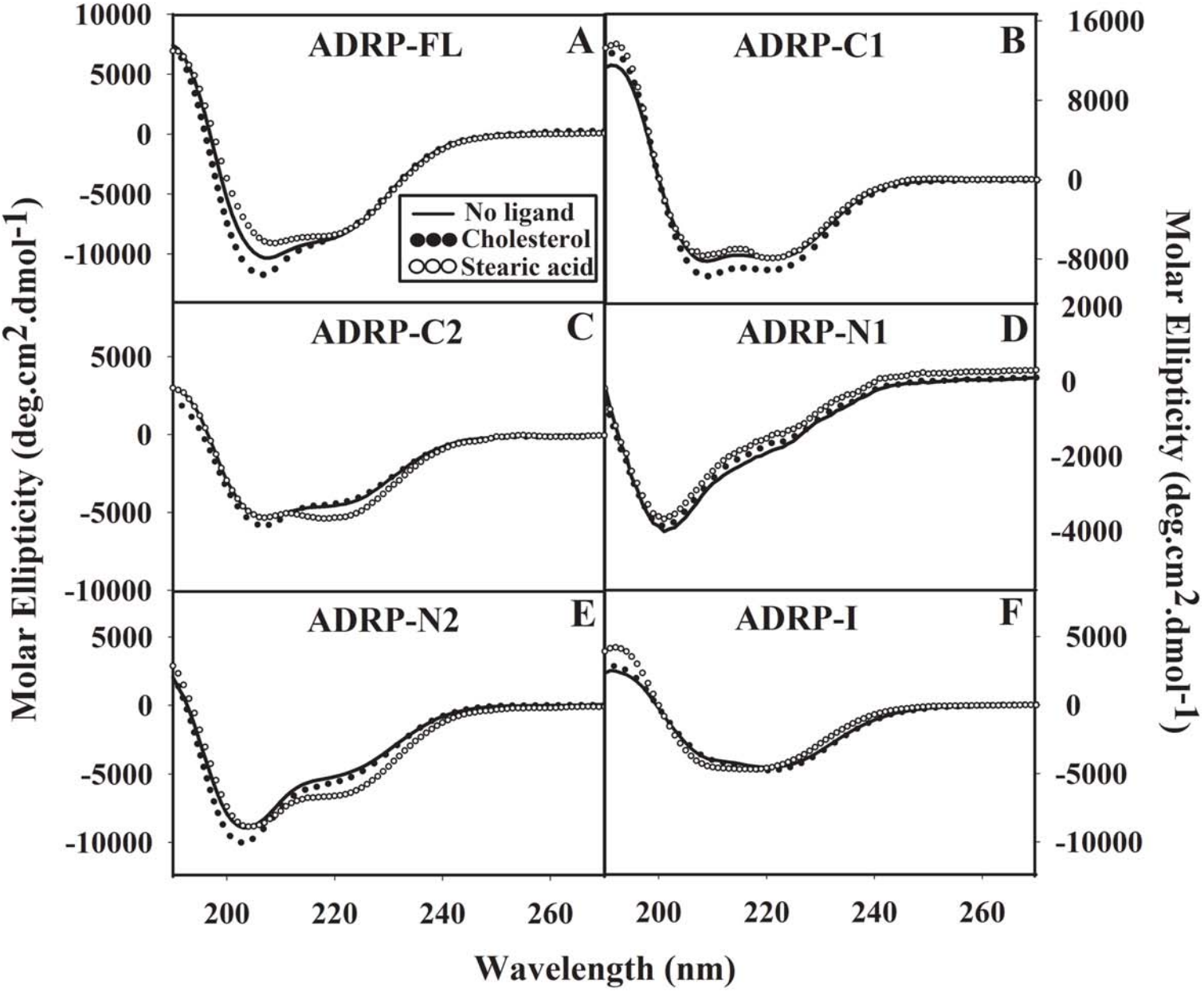
ADRP-FL
A
ADRP-C1
B
ADRP-C2
C
ADRP-N1
D
ADRP-N2
E
ADRP-I
F
No ligand
Cholesterol
Stearic acid
Molar Ellipticity (deg.cm2.dmol-1)
Molar Ellipticity (deg.cm2.dmol-1)
Wavelength (nm)
10000
5000
0
-5000
-10000
16000
8000
0
-8000
2000
0
-2000
-4000
200
220
240
260

Figure 7A

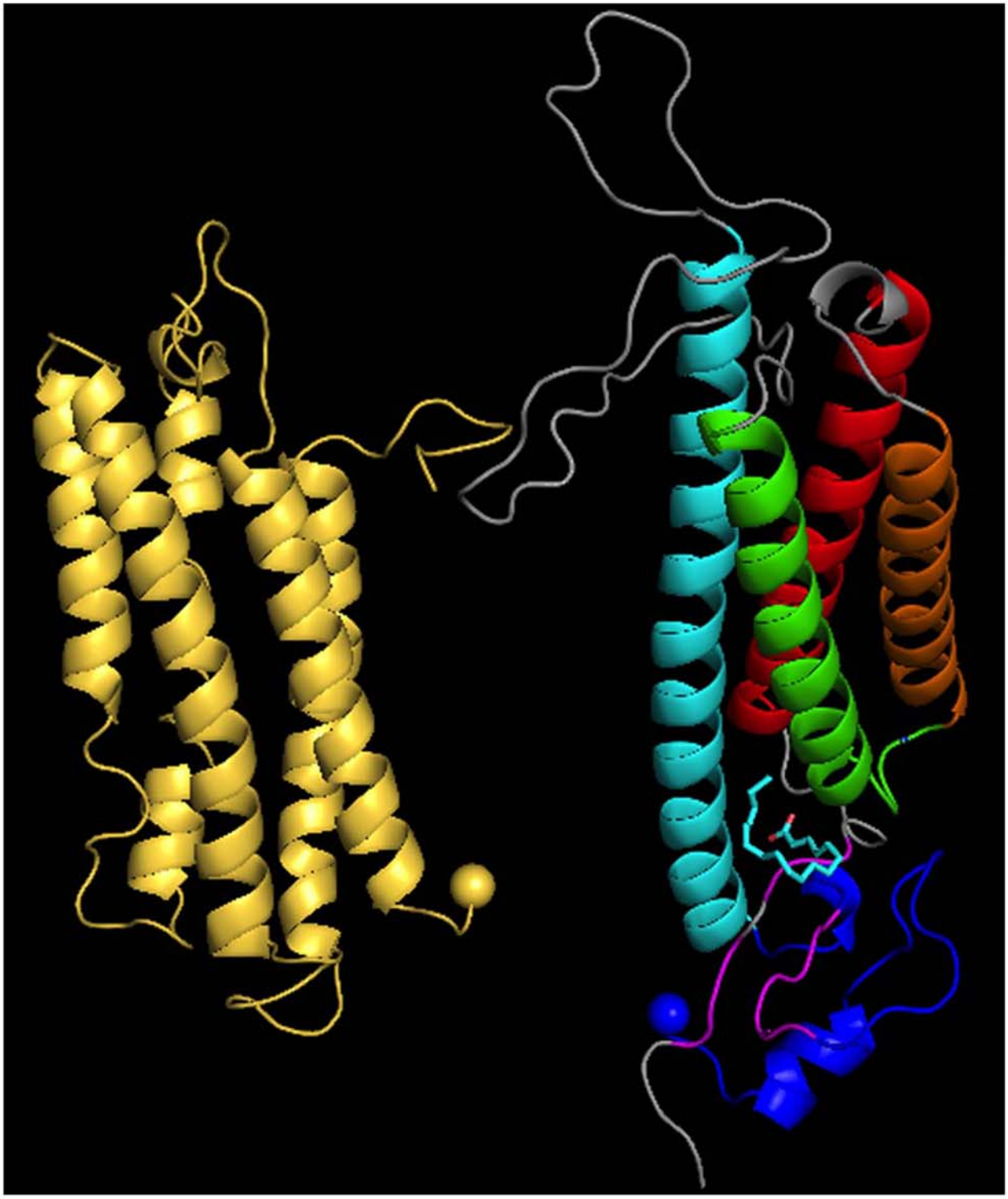

Figure 7B

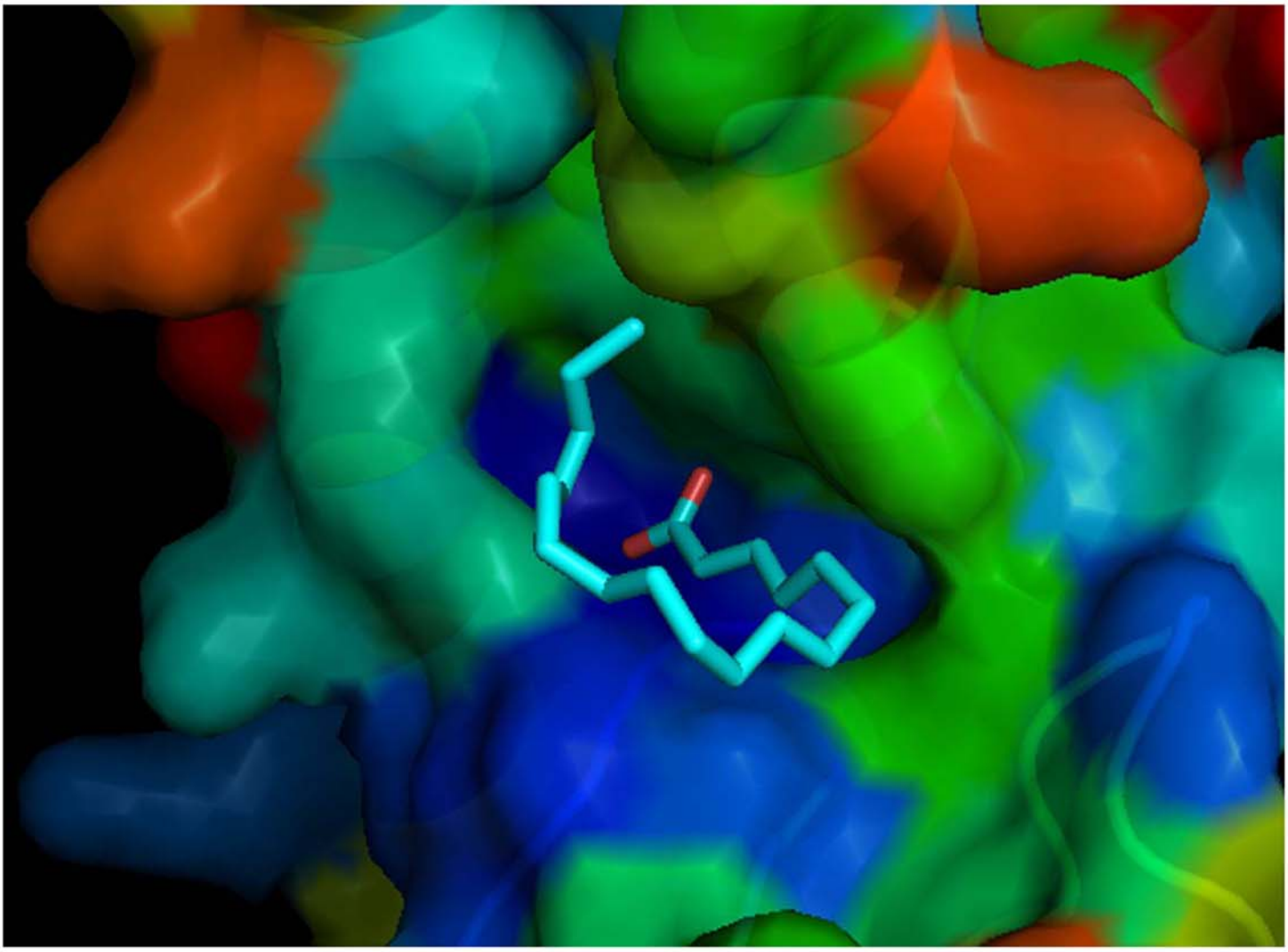

Figure 7C

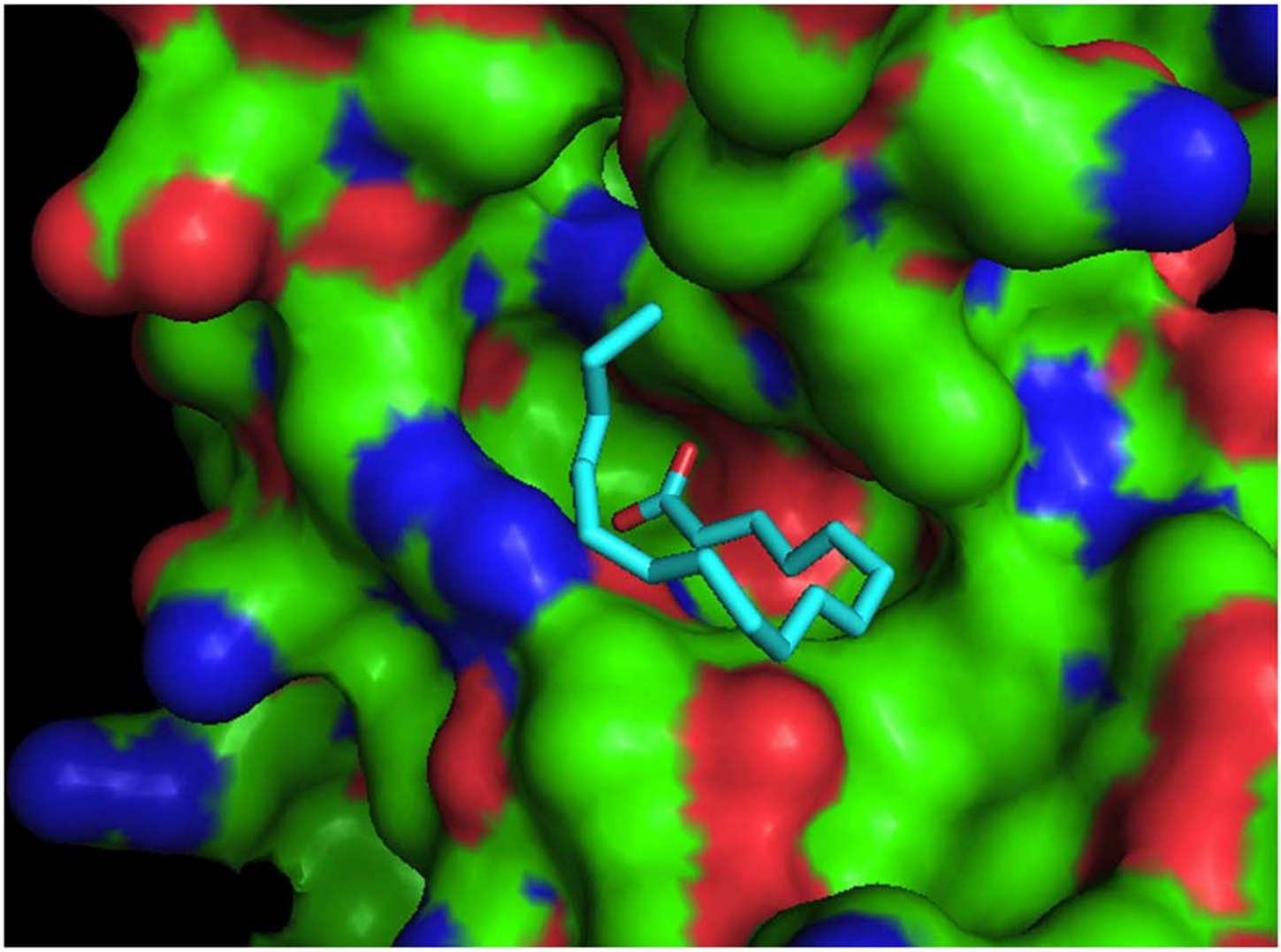

Figure 7D